CHALMERS
UNIVERSITY OF TECHNOLOGY

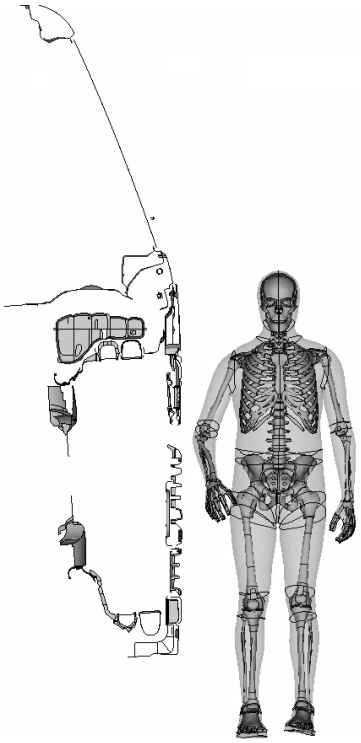

Evaluation of Pedestrian Injury Risks in Truck Frontal Impacts

Parametric Evaluation of Pedestrian Injury Risks in Truck Frontal Impacts

Master's Thesis Report

Master's thesis in Mobility Engineering

Vinay Mallikarjun Hiremath

DEPARTMENT OF MECHANICS AND MARITIME SCIENCE
CHALMERS UNIVERSITY OF TECHNOLOGY
Gothenburg, Sweden 2026
www.chalmers.se

Master's thesis in Mobility Engineering, 2026

Evaluation of Pedestrian Injury Risks in Truck Frontal Impact

Parametric Evaluation of Pedestrian Injury Risks in Truck Frontal Impacts

Vinay Mallikarjun Hiremath



CHALMERS
UNIVERSITY OF TECHNOLOGY

Department of Mechanics and Maritime Sciences
Division of Vehicle Safety
Chalmers University of Technology
Gothenburg, Sweden 2026

Parametric Evaluation of Pedestrian Injury Risks in Truck Frontal Impacts

Vinay Mallikarjun Hiremath

© Vinay Mallikarjun Hiremath, 2026.

Supervisor: Johan Iraeus, Division of Vehicle Safety, Chalmers University
Supervisor: Sarah El-Mobader, Volvo Trucks Technology and Industry Division, Accident Research team | Product Safety
Examiner: Johan Davidsson, Division of Vehicle Safety, Chalmers University

Master's Thesis 2026
Department of Mechanics and Maritime Sciences
Division of Vehicle Safety
Chalmers University of Technology
SE-412 96 Gothenburg
Telephone +46 31 772 1000

Cover: 50th Percentile Male VIVA+ Pedestrian Human Body Model in walking posture for pedestrian crash simulation study.

Typeset in LaTeX
Printed by Chalmers Reproservice
Gothenburg, Sweden 2026

Parametric Evaluation of Pedestrian Injury Risks in Truck Frontal Impacts

Vinay Mallikarjun Hiremath
Department of Mechanics and Maritime Sciences
Chalmers University of Technology

Abstract

Pedestrian fatalities involving heavy goods vehicles represent a significant subset of road traffic accidents, yet truck-to-pedestrian collision biomechanics remain relatively less studied than those involving passenger cars. Unlike passenger cars, which typically impact the lower extremities and cause the pedestrian to wrap onto the hood, the vertical, flat front of a truck interacts with the torso or head. This results in full-body kinematics that differ compared with a pedestrian-to-passenger car event.

This thesis aims to investigate the influence of truck ground height and impact speed on pedestrian injury risks during the primary impact of a frontal truck-to-pedestrian collision.

A parametric finite element study was conducted using the VIVA+ v2.0.1 50th percentile male Human Body Model, aimed at repositioning according to the Euro NCAP TB024 walking posture using the cable-driven Marionette method. Parametric simulations were performed across four truck heights and two impact speeds, using both the VIVA+ 50%ile HBM and a standard Euro NCAP headform impactor.

Simulations were executed in LS-DYNA, with pre- and post-processing in ANSA v2025.2.0 and META v2025.2.0. Injury outcomes were evaluated for the head and brain (HIC15 and DAMAGE), cervical spine (C1 - C7 forces and moments), thorax (rib fracture probability), and lower extremities (femur and tibia fracture risk).

The results indicate that no single ground height minimizes injury risk across all body regions simultaneously. Increasing the height of the simplified truck model reduces the head and neck injury risks but increases the lower extremities and thorax injury risks.

Keywords: Pedestrian safety, Vulnerable road users, HGVs, VIVA+, Human Body Model, Parametric evaluation.

Acknowledgements

This Master's Thesis was carried out at the Department of Mechanics and Maritime Sciences, Chalmers University of Technology and in collaboration with Volvo Group Trucks Technology

I express my sincere gratitude to my supervisors, Johan Iraeus at the Division of Vehicle Safety, Chalmers University of Technology, and Sarah El-Mobader at Volvo Group Trucks Technology, for their constant guidance, support, patience, and valuable feedback throughout the thesis.

I would like to acknowledge Kristian Holmquist and all members of the product safety team at Volvo for this thesis opportunity and their valuable insights and feedback on my thesis.

I would also like to acknowledge the Division of Vehicle Safety at Chalmers University of Technology for providing access to the computational resources and simulation tools used in this study.

Finally, I would like to thank my family and friends for their patience, encouragement, and support throughout my time as a student. This work would not have been possible without them.

Vinay Mallikarjun Hiremath, Gothenburg, August, 2026

List of Acronyms

Below is the list of acronyms that have been used throughout this thesis, listed in alphabetical order:

AIS	Abbreviated Injury Scale
COG	Center of Gravity
DAMAGE	Diffuse Axonal Multi-Axis General Evaluation
Euro NCAP	European New Car Assessment Program
FEA	Finite Element Analysis
FEM	Finite Element Methods
FMVSS	Federal Motor Vehicle Safety Standards
FCR	Family Car
HBM	Human Body Model
HGV	Heavy Goods Vehicle
HIC15	Head Injury Criterion
IARV	Injury Assessment Reference values
IRC	Injury Risk Curve
MPV	Multi-purpose Vehicle
PMHS	Post Mortem Human Subjects
RDS	Roadster
SUV	Sports utility Vehicle
TB024	Euro NCAP Technical Bulletin 2024
YO	Years Old

Contents

List of Acronyms **ix**

Nomenclature **xi**

List of Figures **xiii**

List of Tables **xvii**

1 Introduction **1**
1.1 Background . . . 1
1.2 Literature Study . . . 2
1.2.1 Real World Accident Data . . . 2
1.2.2 Impact velocity and Injury Distribution . . . 2
1.2.3 Environmental Factors . . . 3
1.2.4 Demographics . . . 3
1.3 Unexplored Area of Research . . . 4
1.4 Purpose . . . 4
1.5 Truck Safety Features . . . 5
1.6 Research Questions . . . 5
1.7 Thesis Outline . . . 6

2 Theory **7**
2.1 Injury Criteria and Virtual Tools for Evaluation . . . 7
2.1.1 Head . . . 7
2.1.1.1 Head Injury Criterion (HIC) . . . 7
2.1.1.2 DAMAGE . . . 8
2.1.2 Neck . . . 8
2.1.2.1 Neck Injury Modes . . . 9
2.1.2.2 The Normalized Neck Injury Criterion (N_{ij}) . . . 9
2.1.2.3 Neck Injury Risk . . . 10
2.1.2.4 Neck Forces and Moments . . . 10
2.1.3 Thorax (Rib Fracture Risk) . . . 11
2.1.4 Lower Extremities . . . 12
2.1.4.1 Femur fracture risk . . . 12
2.1.4.2 Tibia fracture risk . . . 13

3 Methods **15**

3.1 Human Body Model . . . 15
3.1.1 VIVA+ 50th %ile HBM Repositioning . . . 15
3.1.1.1 Global transformation . . . 17
3.1.1.2 Marionette Method . . . 17
3.1.1.3 Kinematic Stabilization and Damping . . . 18
3.1.1.4 Simulation Termination and Validation . . . 19
3.2 HeadForm . . . 20
3.3 Simplified Truck Model . . . 21
3.4 Parametric Study and Simulation Setup . . . 21

4 Results **23**
4.1 Crash Kinematics . . . 23
4.2 Head . . . 24
4.3 Neck . . . 29
4.3.1 Force . . . 29
4.3.2 Moment . . . 30
4.4 Thorax . . . 32
4.5 Lower Extremities . . . 34

5 Discussion **37**
5.1 Head and Brain Injury . . . 37
5.1.1 Effect of Simplified Truck Model Height and Impact Speed . . . 37
5.1.2 Comparison Between VIVA+ 50%ile HBM and Headform Impactor . . . 38
5.2 Neck . . . 38
5.3 Thorax . . . 39
5.4 Lower Extremities . . . 40
5.5 Overall Injury Risk . . . 41
5.6 Conclusion . . . 41
5.6.1 Head and Brain Injury: . . . 41
5.6.2 Neck Loading . . . 41
5.6.3 Rib fractures . . . 41
5.6.4 Lower Extremity fractures . . . 42
5.6.5 Overall Conclusion . . . 42
5.7 Future Work . . . 43
5.8 Use of AI . . . 44

Bibliography **45**

A Appendix **I**
A.1 Head Results . . . I
A.1.1 HBM head crash kinematics . . . I
A.1.2 Headform crash kinematics . . . III
A.1.3 Head COG Resultant acceleration and DAMAGE Compilation . . . VI
A.2 Neck Results . . . VIII
A.2.1 Neck forces . . . VIII
A.2.2 Neck Moments . . . X

List of Figures

1.1 Distribution of fatalities over 5-year age categories, by transport mode, in the EU27 (2011-2020); Image Courtesy of European Road Safety Observatory report - 2023 4

2.1 Side View of the Cervical Spine (This image is taken from META results generation tool and enhanced using AI to add labels) 9
2.2 The Sled test alternative neck injury criteria in FMVSS 208 in 1999 [25] 11
2.3 Left and Right Femur and Tibia with impact direction of simplified truck model 12

3.1 VIVA+ v2.0.1 50th %ile male standing posture human body model . 16
3.2 Reference skeleton provided in TB024 certification pack [24] 16
3.3 The generic TB024 reference skeleton model superimposed onto the VIVA+ 50th %ile HBM to determine target coordinates. 18
3.4 Detailed view of the right arm articulation setup, highlighting the cables and viscous dampers. 18
3.5 The final walking posture of the VIVA+ 50th %ile HBM achieved after the 300 ms transient simulation. 19
3.6 Comparison of the four parametric ground heights of the simplified truck model in front of the VIVA+ 50th %ile HBM 22
3.7 Comparison of the four ground heights of the simplified truck model in front of the headform. 22

4.1 Full Body Crash kinematics of the VIVA+ 50th %ile HBM for 320 mm simplified truck model height at 40 km/h 24
4.2 Head impact locations of VIVA+ 50th %ile HBM across all the simplified truck model heights 25
4.3 Close-up head kinematics of the VIVA+ 50th %ile HBM for 120 mm simplified truck model height at 40 km/h 25
4.4 Close-up kinematics of the headform impact for 120 mm simplified truck model height at 40 km/h. 25
4.5 HIC and DAMAGE across all four simplified truck model heights at 40 km/h and 24 km/h. 27
4.6 Comparison of Head and Brain Injury Risks from VIVA+50th %ile HBM and Head Injury Risk for headform 28

4.8 Neck Moment (Nm) magnitudes at the C6 and C7 cross-sections across 40 km/h and 24 km/h. 30
4.9 Distribution graphs comparing the rib fracture risks across all simplified truck model ground heights for the 40 km/h and 24 km/h impact scenarios. 32
4.10 Total number of fractured ribs probability across all the simplified truck model ground heights at 40 km/h and 24 km/h for 25 YO. . . . 33
4.11 Number of fractured ribs by age group across varying simplified truck model heights for 40 km/h and 24 km/h impact speeds. 34
4.12 Comparison of 99% Strain fracture risks for the Femur and Tibia across different simplified truck model ground heights. 35

5.1 Color gradient scale for full-Body injury severity maps ranging from 0.0 (low risk) to 1.0 (high risk). 42
5.2 Full-body injury severity maps illustrating injuries across all four simplified truck model heights at 40 km/h and 24 km/h. 43

A.1 Close-up head kinematics of the VIVA+ 50th %ile HBM for 120 mm simplified truck model height at 24 km/h I
A.2 Close-up head kinematics of the VIVA+ 50th %ile HBM for 120 mm simplified truck model height at 40 km/h I
A.3 Close-up head kinematics of the VIVA+ 50th %ile HBM for 220 mm simplified truck model height at 24 km/h I
A.4 Close-up head kinematics of the VIVA+ 50th %ile HBM for 220 mm simplified truck model height at 40 km/h II
A.5 Close-up head kinematics of the VIVA+ 50th %ile HBM for 320 mm simplified truck model height at 24 km/h II
A.6 Close-up head kinematics of the VIVA+ 50th %ile HBM for 320 mm simplified truck model height at 40 km/h II
A.7 Close-up head kinematics of the VIVA+ 50th %ile HBM for 420 mm simplified truck model height at 24 km/h II
A.8 Close-up head kinematics of the VIVA+ 50th %ile HBM for 420 mm simplified truck model height at 40 km/h III
A.9 Close-up kinematics of the headform impact for 120 mm simplified truck model height at 24 km/h. III
A.10 Close-up kinematics of the headform impact for 120 mm simplified truck model height at 40 km/h. III
A.11 Close-up kinematics of the headform impact for a 220 mm simplified truck model height at 24 km/h. IV
A.12 Close-up kinematics of the headform impact for a 220 mm simplified truck model height at 40 km/h. IV
A.13 Close-up kinematics of the headform impact for 320 mm simplified truck model height at 24 km/h. IV
A.14 Close-up kinematics of the headform impact for a 320 mm simplified truck model height at 40 km/h. V
A.15 Close-up kinematics of the headform impact for 420 mm simplified truck model height at 24 km/h. V

A.16 Close-up kinematics of the headform impact for 420 mm simplified truck model height at 40 km/h. V
A.17 Comparison of Head COG Resultant Acceleration across varying simplified truck model heights at 40 km/h and 24 km/h impact speeds for VIVA+ 50th %ile HBM. VI
A.18 Comparison of Head COG Resultant Acceleration across varying simplified truck model heights at 40 km/h and 24 km/h impact speeds for headform VI
A.19 Comparison of the Head DAMAGE metric across varying simplified truck model heights at 40 km/h and 24 km/h impact speeds for VIVA+ 50th %ile HBM. VII
A.20 Comparison of Neck Force (kN) magnitudes at the C1 through C3 cross-sections across 40 km/h and 24 km/h impact speeds. VIII
A.21 Comparison of Neck Moment (Nm) magnitudes at the C1 through C3 cross-sections across 40 km/h and 24 km/h. X
A.21 Comparison of Neck Moment (Nm) magnitudes at the C4 through C7 cross-sections across 40 km/h and 24 km/h. (Continued) XI

List of Tables

2.1 Coefficients used in the DAMAGE-based AIS 2+ injury risk function (TB035 [32]). 8
2.2 Independent peak neck force and moment limits for the Hybrid III 50th percentile male ATD 10

3.1 Validation of the repositioned VIVA+ 50th %ile HBM posture against Euro NCAP TB024 protocol targets. 20
3.2 Detailed parametric simulation matrix. 21

4.1 AIS 2+ injury risks for HIC and DAMAGE using equations 2.2 and 2.3 across all four simplified truck model ground heights at 40 km/h and 24 km/h for **VIVA+ 50% ile HBM.** 26
4.2 AIS 2+ injury risks for HIC using equation 2.2 across varying simplified truck model ground heights at 40 km/h and 24 km/h for **headform.** 26
4.3 Peak N_{ij} Values and AIS 3+ Injury Risk for Mid and Lower Cervical Levels at 24 km/h and 40 km/h 31
4.4 Fracture risks from 99% Strain for the Femur Shaft and Tibia across varying simplified truck model ground heights at 24 km/h and 40 km/h (Left is the Non-struck side, and Right is the Struck side) . . . 34

1
Introduction

The transport industry is experiencing an increasing prevalence of Heavy Goods Vehicles (HGVs) on public roads, driven by global demand for transport [2] [3]. Research on pedestrian protection focuses predominantly on passenger cars; however, collisions involving heavy goods vehicles are also of considerable importance [16]. The presence of these vehicles on public roads poses a risk to vulnerable road users.

In the event of an accident (see section 1.2, literature study for detailed statistics), vulnerable road users, specifically pedestrians, are at substantial risk due to factors such as the high mass of a truck, increased blind spots, and high likelihood of being run over [5]. Unlike passenger cars, where the pedestrian often wraps around the hood, vehicles with tall, blunt front ends prevent this rotation and increase injury severity [7]. This thesis investigates the biomechanics of such collisions through advanced finite element simulations.

Current research needs to deepen the understanding of Injury Risks and the kinematics of the human body's behaviour in a collision with a truck, including what parameters influence these injury Risks. Specifically, there is a need to isolate and analyse the injuries by the primary impact (pedestrian vs. truck), to gain knowledge in the area of truck-to-pedestrian collisions.

1.1 Background

Most modern passenger cars are designed with a sloped hood. In a passenger car-to-pedestrian impact, the design of the passenger car allows the pedestrian to rotate, distributing impact forces across a larger surface area over a longer duration. A relatively short hood, a large hood angle, a large windshield angle, and a wide windshield reduced the risks of fatal or severe head injuries to pedestrians [6]. But during a truck-to-pedestrian impact, where the truck has a vertical, flat, blunt front-end geometry, research has shown this geometry may result in high likelihood of severe injuries for pedestrians [7]. This interaction results in a high likelihood of the pedestrian being projected forward which may result in a secondary impact with the ground, with a likelihood of being run over.

1.2 Literature Study

1.2.1 Real World Accident Data

Worldwide, vehicle impacts with pedestrians constitute the most frequent cause of traffic-related fatalities; as a result, knowledge about pedestrian impacts is essential to the reduction of fatalities and injuries for vulnerable road users [19]. According to the WHO Global Status Report on Road Safety 2023, road traffic deaths have fallen by 5% since 2010 to approximately 1.19 million annually. Pedestrians account for 23% of all global road traffic fatalities, approximately 274,000 deaths per year, and pedestrian fatalities actually rose 3% between 2010 and 2021 despite overall reductions in road deaths [9].

In the United States, the number of pedestrian fatalities has increased since 2009, leading to a five-year average of 6,502 fatalities recorded between 2017 and 2021, during which pedestrians accounted for 16% to 17% of all traffic fatalities (National Center for Statistics and Analysis (NCSA),2023) [10]. In 2023, a total of 7,314 pedestrian fatalities were reported, among these, 367 (5%) were involved heavy goods vehicles [8], consistent with the longer-term trend reported by Chong [11], who highlighted that between 2006 and 2015, 2,315 of 47,789 pedestrian fatalities (4.8%) resulted from collisions involving heavy goods vehicles, with over 674,000 pedestrian injuries reported by NHTSA during the same period. Similarly, in Asia, where mixed traffic conditions and high population densities are prevalent, pedestrian vulnerability is high. In Japan, 35.2% of total traffic fatalities according to the Transportation Authority Police 2010 pedestrians were fatally injured. In China, more than 23,000 pedestrian were killed in road traffic accidents in 2006 (Traffic Administration Bureau of China, 2007), accounting for 26% of their total traffic fatalities [15].

Despite constituting a relatively small proportion (6%) of total vehicle mileage in a country like Sweden, trucks appear in 15%–20% of all road fatalities [12]. This is reinforced by European data indicating that almost 30% of those who were fatally injured in 2013 in road accidents involving buses were with pedestrians and 17% involved heavy goods vehicles [13]. In Germany, Malczyk and Bende [14] analyzed 2015 crash data for trucks over 12 tonnes and highlighted that while collisions with pedestrians and bicyclists accounted for 4% and 9% of crashes, respectively, these vulnerable road users comprised 26% of the total fatalities.

1.2.2 Impact velocity and Injury Distribution

Fatalities involving Heavy goods vehicles (HGVs) are strongly correlated with impact velocity and the vehicle's frontal geometry. Matsui et al. [15] quantified this risk, reporting that at low impact velocities (less than 30 km/h), the fatality risk for a pedestrian struck by a heavy-duty truck (gross vehicle weight greater than 12 tonnes) is 10.6%, compared to 0.5% for sedans. At medium speeds (31–60 km/h), the risk for pedestrian fatality for heavy-duty trucks and sedans increases to 25.4%

and 10.7% respectively.

The predominant crash scenario is frontal impact, representing 67% of truck-to-pedestrian accidents [13]. Feist et al. [16] identified the head as the most severely injured body region (average AIS 3.1), followed by the abdomen/pelvis (average AIS 2.9) and thorax (average AIS 2.1). The study also highlighted that 69% of sustained head injuries in HGV collisions are attributed to rotational acceleration mechanisms, compared to only 21% caused by translational forces [16].

1.2.3 Environmental Factors

Malczyk and Bende [14] analyzed that a data sample provided by the German Insurance Accident database on truck accidents occurring between 2007 and 2012 included a total of 39 crashes involving 43 pedestrians. A majority of crashes occurred in built-up areas (pedestrians injured: n=35; 89%) and during daylight (pedestrians injured: n=39; 91%). Almost half of the cases (cases: n = 21; 49%) occurred on stretches of road. The truck was going straight in the large majority of cases where a pedestrian was struck. 40% of 43 pedestrians were run over, five of them with fatal consequences. Often, the truck collided with a pedestrian when accelerating from a stationary position. In 11 cases (26% of 39), traffic was significantly less frequently controlled by traffic lights at junctions or crosswalks in pedestrian accidents

1.2.4 Demographics

From the same study by Malczyk and Bende [14], females account for 58% of total pedestrian fatalities (25 of 43 pedestrians). Pedestrians averaged 57.8 years of age (median 61 years). 50.7% of all pedestrians fatally injured were persons aged 65 and older.
According to the European Commission (2021) Facts and Figures Pedestrians. European Road Safety Observatory, Brussels, European Commission, Directorate General for Transport, [4], in 2020, almost 1 in 2 pedestrian fatalities was a person aged 65 or older, and people between 15 and 24 years had a lower share in the number of pedestrian fatalities (5% in 2020) than in the total number of road fatalities (14% in 2020)

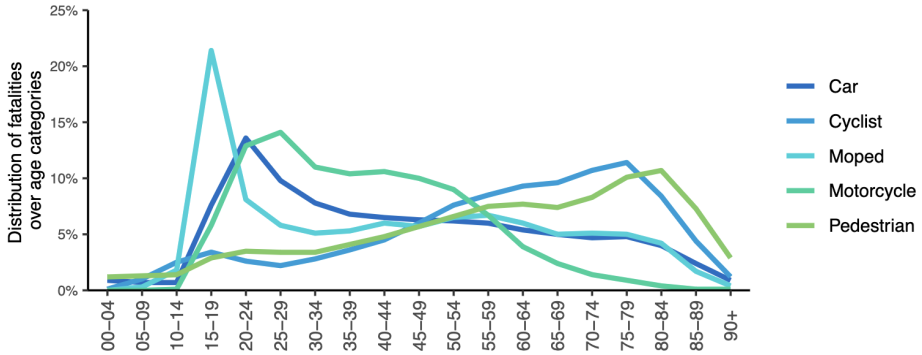

Figure 1.1: Distribution of fatalities over 5-year age categories, by transport mode, in the EU27 (2011-2020); Image Courtesy of European Road Safety Observatory report - 2023

From the same report [4], referencing the statistics in Figure 1.1, the mortality rate for pedestrians over the age of 65 is three times higher than for those between the ages of 25 and 64, and seven times higher than for individuals under the age of 25.

Similarly, from the US NHTSA Data, [10], the age groups (60 - 64 and 65 - 70) make up the highest percentage of pedestrian fatalities (23%) among the other age groups. Older pedestrians are more likely to suffer from fatal injuries in truck-to-pedestrian impacts due to the inherent fragility associated with the aging process. In the 2023 NHTSA report mentioned in section 1.2.1, among the 7,314 pedestrian fatalities, 5,148 were male compared to 2,126 female, a ratio of approximately 2.4:1, a pattern that is consistent across years and reflects broader trends in traffic safety research.

1.3 Unexplored Area of Research

Current vehicle-pedestrian research, regulatory testing, and development of safety measures are mainly focused on passenger cars. Consequently, existing safety protocols are optimised based on evaluations developed from a kinematic study of generic vehicle models representing standard passenger cars (which includes FCR, MPV, RDS, and SUVs) [19, 21]. However from the real-world statistical data, it is seen that from the study by Matsui in Japan[15], collisions with heavy goods vehicles are more severe than those involving passenger cars.

However, there is a gap in the literature regarding the detailed biomechanical evaluation in truck-to-pedestrian crashes. Specifically, there is a need to understand how various crash parameters influence pedestrian injuries during primary impact.

1.4 Purpose

This thesis aims to investigate the influence of the parameters of a simplified truck model (impact speeds and heights) and the injury outcomes through Finite Element

Analysis using the VIVA+ 50th %ile male Human Body Model (HBM) in truck-to-pedestrian collision scenarios. This analysis will focus on Head Injury Criteria (HIC), brain tissue damage metric - Diffuse Axonal, Multi-Axis, General Evaluation (DAMAGE), neck loads (Force and Moment), rib, femur, and tibia fracture risks. Furthermore, the research seeks to compare the results (specifically the HIC) from VIVA+ 50th %ile HBM with the standard headform impactor.

1.5 Truck Safety Features

In order to address the injuries and fatalities, vehicle safety systems for pedestrian have been classified mainly into active and passive safety systems. The active safety systems mainly focuses detection of potential collisions and take preventive actions before impact. In the context of pedestrian collisions, these systems rely on real-time data from sensors to identify pedestrians in the path of the vehicles and deploy various safety systems, such as applying emergency brakes and alerting the driver with auditory or visual alerts to mitigate the severity of the potential collision. In contrast, passive safety systems focus on reducing the injury severity once the collision has occurred. These systems help in absorbing and distributing impact forces. Examples include deformation zones and specially designed vehicle front structures that are intended to reduce the impact on pedestrians [31].

Given the scope of the thesis, the focus will be on passive safety aspects in pedestrian protection.

1.6 Research Questions

The main research questions that have been focused on addressing in this thesis are:

1. How do truck height and impact speed influence pedestrian injury Risks, and full-body kinematics of a VIVA+ 50th %ile HBM during the primary impact of a truck-to-pedestrian frontal collision?
2. How do the head injury predictions from the VIVA+ 50th %ile HBM compare with those from the standard Euro NCAP headform impactor across the same parametric conditions?

1.7 Thesis Outline

The thesis is structured into five chapters. Following this introduction covering a review of real-world accident statistics, the biomechanics of truck-to-pedestrian collisions, Chapter 2 presents the theoretical background and the injury criteria used to evaluate head, neck, thorax, and lower extremity injury risk. Chapter 3 focuses on the simulation setup and methodology, detailing the repositioning of the VIVA+ 50th %ile HBM into the Euro NCAP TB024 walking posture, the simplified truck model used for simulations, the headform impactor setup, and the parametric simulation matrix. Chapter 4 presents the compilation of all the results from all simulations for each body region. Chapter 5 discusses the findings in the context of injury risks, addresses each research question, draws conclusions on the influence of the height of the simplified truck model and impact speed on pedestrian injury outcomes, and identifies scope for future work.

2

Theory

2.1 Injury Criteria and Virtual Tools for Evaluation

2.1.1 Head

Head injury in this study was evaluated using acceleration response-based criteria: the Head Injury Criterion (HIC), which is derived from the translational acceleration of the head. While HIC captures translational head acceleration, it does not account for rotational kinematics — a commonly cited limitation of the criterion [34]. To address this limitation, the DAMAGE criterion is additionally used in this study. Diffuse Axonal, Multi-Axis, General Evaluation (DAMAGE) is a maximum principle strain (MPS) response of a mid-sized FE brain model-based brain injury metric that accounts for rotational velocities of head motion [34]. These two metrics were extracted for every simulation to capture both skull and brain injury risk, and the diffuse axonal injury risk associated with rotational loading.

2.1.1.1 Head Injury Criterion (HIC)

The Head Injury Criterion (HIC) originates from the work of Gadd (1961) [35], who used the Wayne State Tolerance Curve (WSTC) to develop the severity Index, which was later refined by Versace (1971) [37] into a measure of average acceleration correlating with the WSTC [34]. HIC is used to indicate the severity of head injury by correlating it with the Abbreviated Injury Scale (AIS). In 1998, NHTSA introduced HIC_{15}, which is evaluated over a maximum time interval of 15 ms, now in force under the current version of Federal Motor Vehicle Safety Standard (FMVSS) 208 [34]. HIC_{15} is computed based on the following expression:

$$HIC = \max_{t_1,t_2} \left[\left(\frac{1}{t_2 - t_1} \int_{t_1}^{t_2} a(t)\, dt \right)^{2.5} (t_2 - t_1) \right] \tag{2.1}$$

where t_1 and t_2 are any two arbitrary time points during the acceleration pulse, in seconds [34]. In this study, HIC_{15} was used and extracted from the resultant head acceleration signal in META for each simulation. Figure A.17 shows the compilation of resultant head COG acceleration plots for both 40 km/h and 24 km/h simulations. To determine the relationship between HIC and the risk of AIS 2+ Head injury, the probability of skull fracture (AIS $\geq$ 2) is given by [34]:

$$P(AIS\ 2+) = N\left(\frac{\ln(HIC) - \mu}{\sigma}\right) \tag{2.2}$$

where $N(\cdot)$ denotes the cumulative normal distribution, $\mu = 6.96352$, and $\sigma = 0.84664$ [34]. HIC was specifically correlated to skull fracture through this statistical relationship, rather than to brain injury or other head injury types [34].

2.1.1.2 DAMAGE

Finite element brain models have been increasingly used to predict strain-based brain injury risk directly, using metrics such as maximum principal strain (MPS), shear strain, and strain rate [34]. DAMAGE is one such criterion, based on a second - order model analogous to a multi-body mechanical system. DAMAGE uses the directionally dependent angular acceleration time histories from a head impact to estimate the magnitude of brain deformation via MPS [38]. DAMAGE was extracted from each simulation to capture rotational brain injury risk from META. To convert the DAMAGE value into an AIS 2+ brain injury probability, the risk function defined in the Euro NCAP Technical Bulletin 035 (TB035) [32] was applied:

$$P(AIS\ 2+) = 1 - e^{\left(-e^{\left(\frac{1}{b}\ln(y+c) - \frac{a}{b}\right)}\right)} \tag{2.3}$$

where y is the DAMAGE value extracted from the calculations, and a, b, c, and d are empirically derived coefficients corresponding to the scale, shape, intercept, and slope parameters of a Weibull-based injury risk distribution. The coefficient values used in this study, as specified in TB035, are listed in Table 2.1.

Table 2.1: Coefficients used in the DAMAGE-based AIS 2+ injury risk function (TB035 [32]).

Parameter	Value
Scale (e^a)	0.459
Shape ($1/b$)	3.875
Intercept (c)	0.017
Slope (d)	0.957

Together, HIC and DAMAGE allow the head injury risk in this study to be assessed from both a translational and a rotational perspective, providing a more complete picture of head and brain injury risk.

2.1.2 Neck

Given the neck's primary role as a link between the head and the rest of the body, the internal loading at each cervical level (C1 through C7) was extracted to identify peak force and moment magnitudes at both speeds.

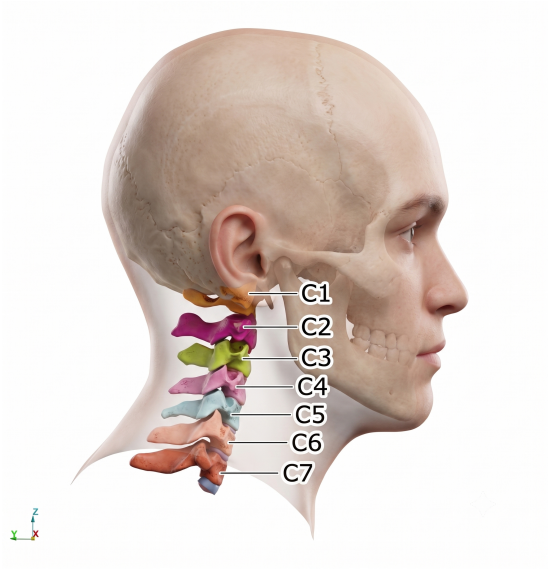

Figure 2.1: Side View of the Cervical Spine (This image is taken from META results generation tool and enhanced using AI to add labels)

The above figure 2.1 illustrates the cervical spine, consisting of the seven vertebrae (C1 through C7) that form the neck region, highlighting the anatomical positioning and vertical arrangement of these individual bones, which support the weight of the head and allow for its range of motion.

2.1.2.1 Neck Injury Modes

The neck exhibits the following predominant injury modes: [34]

- N_{TE}: Tension-Extension
- N_{TF}: Tension-Flexion
- N_{CE}: Compression-Extension
- N_{CF}: Compression-Flexion
- N_{lat}: Lateral Bending.

2.1.2.2 The Normalized Neck Injury Criterion (N_{ij})

The Normalized Neck Injury Criterion (N_{ij}) is an evaluation metric utilized to predict the probability of cervical spine injuries [25]. Originally formulated by the National Highway Traffic Safety Administration (NHTSA) for use with Anthropomorphic Test Devices (ATDs), the criterion is defined as a linear combination of tension/compression and flexion/extension moments, where the 'i' represents the axial load (tension and compression) and 'j' represents the sagittal plane bending moment (flexion or extension) [26]

The normalized neck injury criteria N_{ij}, calculated according to the equation as:

$$N_{ij} = \frac{F_z}{F_{int}} + \frac{M_y}{M_{int}} \tag{2.4}$$

Where:

- F_z is the axial load
- F_{int} is the normalized critical intercept value of load according to the specific dummy corresponding to F_z
- M_y is the transient sagittal bending moment
- M_{int} is the normalized critical intercept value for moment according to the specific dummy corresponding to M_y

Table 2.2 summarizes the critical intercept values for the 50th %ile male Hybrid III dummy developed using cadaveric test data [25].

Table 2.2: Independent peak neck force and moment limits for the Hybrid III 50th percentile male ATD

Dummy Type	**Tension (N)**	**Compression (N)**	**Flexion (Nm)**	**Extension (Nm)**
Hybrid III 50th %ile Male	3600	3600	410	125

The N_{ij} threshold value of 1.0 is designated as the critical performance limit, corresponding to a 15% risk of sustaining an AIS 3+ neck injury [25].

2.1.2.3 Neck Injury Risk

The probability of neck injury risk is calculated using the (N_{ij}) by the equation 2.5 given as:

$$p(AIS \geq 3) = \frac{1}{1 + e^{3.906 - 2.185 Nij}} \tag{2.5}$$

2.1.2.4 Neck Forces and Moments

In addition to the N_{ij} metric, the independent evaluation of peak neck forces and moments is also utilized to assess ATD neck injury risk, specifically within the alternative sled test provisions of Federal Motor Vehicle Safety Standard (FMVSS) 208 [25]. Under these guidelines, the forces and moments recorded by the dummy must remain within the tolerance limits, given by the shaded grey box in Figure 2.2

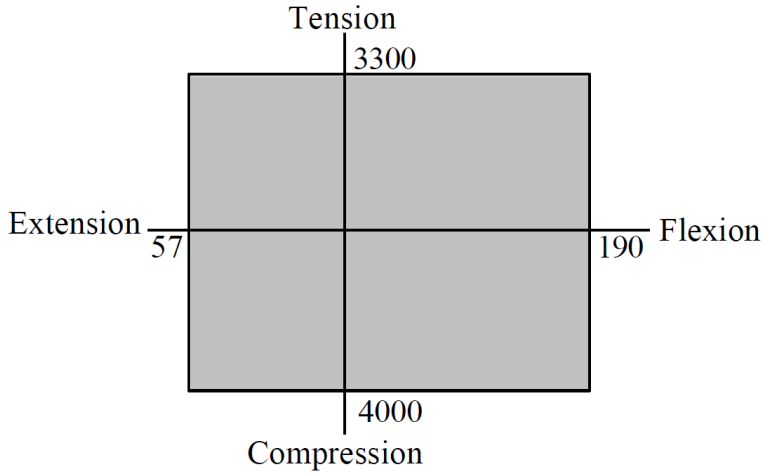

Figure 2.2: The Sled test alternative neck injury criteria in FMVSS 208 in 1999 [25]

2.1.3 Thorax (Rib Fracture Risk)

To assess the risk of rib fracture simulations, the META tool employs a probabilistic framework utilizing a tissue-based, age-adjusted rib fracture risk function developed by Larsson et al.[27]. This injury risk function translates the rib cortical bone strains obtained from the simulations into the fracture probability [27].

This risk function was developed using survival analysis with an accelerated failure time (AFT) model, based on dynamic tensile test data of human rib cortical bone samples spanning a wide age range (17 to 99 years). It employs a log-normal distribution, which was selected over Weibull and log-logistic distributions. The probability of rib fracture as a function of the true strain and the occupant's age is calculated using the following parametric expression [27]:

$$p(\text{fracture}) = \frac{1}{2} + \frac{1}{2}\text{erf}\left(\frac{\ln(\varepsilon) - (\beta_0 + \beta_1 \cdot \text{AGE})}{\sqrt{2} \cdot \alpha}\right) \tag{2.6}$$

Where:

- p(fracture) is the probability of rib cortical bone fracture.
- erf() represents the Gauss error function.
- ln() is the natural logarithm.
- ε is the true strain (logarithmic strain) extracted from the finite element model.
- AGE is the subject's age in years.

The specific distribution parameters for the log-normal distributions are defined as [27]:

- $\boldsymbol{\alpha} = 0.3026$
- $\boldsymbol{\beta_0} = -2.9866$
- $\boldsymbol{\beta_1} = -0.0130$

The negative value of β_1 reflects the age-dependent reduction in rib cortical bone failure strain. The acceleration factor associated with aging is $\exp(\beta_1 \cdot \text{AGE})$; using

the log-normal parameter $\beta_1 = -0.0130$, this corresponds to a **12.2% reduction in failure strain per decade of aging**.
The META tool extracts the peak strain from ribs of the 50%ile VIVA+ HBM. Using Equation 2.6, it calculates the individual fracture risk for each rib based on its specific strain and the occupant's age. These individual risks are then combined using the [28] probabilistic framework to predict the overall probability of sustaining two or more Number of fractured ribs (NFR2+).

2.1.4 Lower Extremities

In vehicle-to-pedestrian collisions, the lower extremities are primarily subjected to lateral loading from the vehicle's front-end structure. For the long bones—specifically the femur shaft and tibia the injury mechanism are fractures [36]. Figure 2.3 shows the direction in which the simplified truck model was impacted the VIVA+ 50%ile HBM, in which the right femur and tibia were the struck side and the left femur and tibia were the non-struck side.

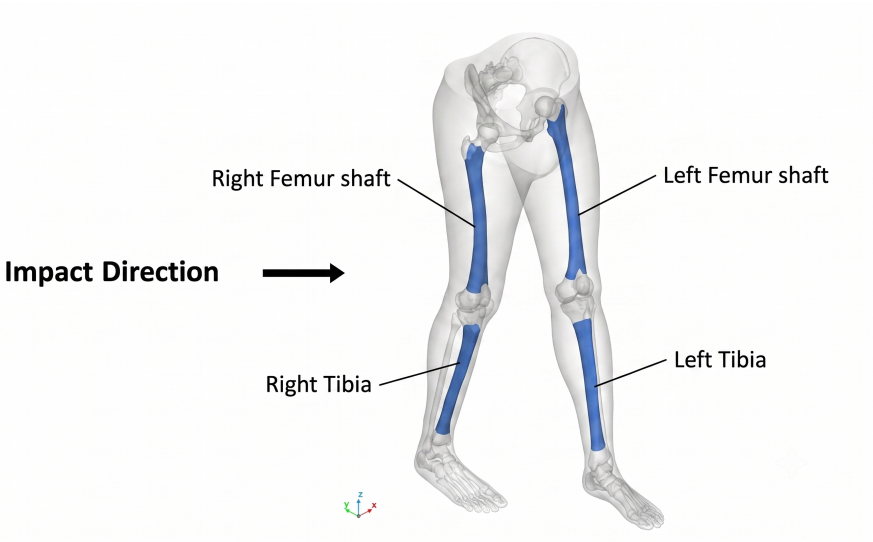

Figure 2.3: Left and Right Femur and Tibia with impact direction of simplified truck model

2.1.4.1 Femur fracture risk

Schubert [29] developed the femur shaft Injury Risk Curve (IRC) by computationally simulating 14 physical bone fracture tests. To define the failure threshold, they used the 99th percentile principal strain (PS99) of the bone at the moment of fracture [29]. PS99 was chosen instead of the absolute maximum strain to prevent the results from being skewed by numerical errors in a single element.

The resulting injury risk for the femur shaft is modeled using a parametric Weibull survival function. The specific Weibull parameters derived for the femur shaft using

the PS99 metric are as follows:

- **Shape factor (k):** 2.7426
- **Scale parameter (λ):** 0.0342

The probability of a femur shaft fracture can therefore be calculated using the standard Weibull cumulative distribution function [29]:

$$P_{\text{fracture}}(\varepsilon_{99}) = 1 - \exp\left(-\left(\frac{\varepsilon_{99}}{\lambda}\right)^{k}\right) \tag{2.7}$$

where ε_{99} represents the 99th percentile principal strain extracted from the finite element cortical bone mesh, λ is the scale parameter (0.0342), and k is the shape factor (2.7426).

2.1.4.2 Tibia fracture risk

Similarly, the tibia shaft Injury Risk Curve (IRC) used in this study was developed by Harden et al. [39] following the same methodology as the femur shaft IRC. Physical tibia bending tests were computationally replicated, and the 99th percentile principal strain (PS99) of the cortical bone at the moment of fracture was used as the failure threshold metric, consistent with the approach used for the femur shaft IRC [29]. PS99 was again chosen over the absolute maximum strain.

The resulting injury risk for the tibia shaft is modelled using a parametric Weibull survival function. The Weibull parameters derived for the tibia shaft using the PS99 metric, as implemented in the VIVA+ post-processing framework in the Dynasaur library [40], are as follows:

- **Shape factor (k):** 5.0819
- **Scale parameter (λ):** 0.0120

The probability of a tibia shaft fracture is calculated using the same Weibull cumulative distribution function as the femur shaft [39]:

$$P_{\text{fracture}}(\varepsilon_{99}) = 1 - \exp\left(-\left(\frac{\varepsilon_{99}}{\lambda}\right)^{k}\right) \tag{2.8}$$

where ε_{99} represents the 99th percentile principal strain extracted from the finite element cortical bone mesh of the tibia, λ is the scale parameter and k is the shape factor as listed above.

3
Methods

In this chapter, the workflow and approach of the study performed, and the implementation of the theories in the previous chapters are presented.

3.1 Human Body Model

In traditional vehicle safety assessments, Anthropomorphic Test Devices (ATDs), or crash test dummies, are the primary tools. However, due to the lack of biofidelity and anatomical resolution with repetitive capabilities, the development of numerical human body models was initiated [23]. The introduction of Technical Bulletin - 2024 (TB024) [22] marks a transitional phase where HBMs are being considered as a complementary tool to traditional ATD-based methods. The TB024 outlines requirements for numerical pedestrian models and simulation setups to ensure that the performance of models and simulation results can be compared fairly [21]. For the simulations in this thesis, the latest version (2.0.1) of the VIVA+ 50th %ile male Human Body Model was selected. The pre-processing and post-processing for the simulations were carried out in BETA CAE systems: ANSA v2025.2.0 and META v2025.2.0, respectively. The FE simulations were conducted using LS-DYNA R12.2.2 MPP.

3.1.1 VIVA+ 50th %ile HBM Repositioning

The 2.0.1 version of VIVA+ 50th %ile male Human Body Model (HBM) is provided in a nominal standing posture. To evaluate truck-to-pedestrian kinematics, the model was repositioned into a standard walking stance according to TB024 before the impact simulation. Figure 3.1 shows the default standing posture of the VIVA+ 50th %ile HBM.



Figure 3.1: VIVA+ v2.0.1 50th %ile male standing posture human body model

The target posture was defined in accordance with the Euro NCAP Technical Bulletin 2024 (TB024) guidelines[22], which require specific limb positioning and joint angles for pedestrian impact testing. To achieve this, a geometric alignment strategy was employed. The TB024 skeleton model in pedestrian position, which was provided with the TB024 certification pack was superimposed onto the baseline VIVA+ 50th %ile HBM by aligning pelvis and spine of both skeletal structures within the ANSA environment. By mapping the nodes of the VIVA+ 50th %ile HBM model to the corresponding joints and extremities of the TB024 skeleton, the exact translational distances and displacements required for the hands, legs, and major joints were defined. Figure 3.2 shows the reference skeleton used from the certification pack on the Euro NCAP website.

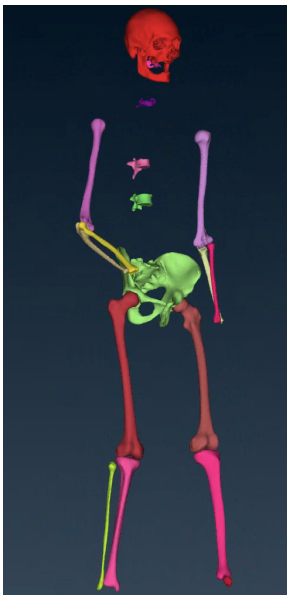

Figure 3.2: Reference skeleton provided in TB024 certification pack [24]

The repositioning was executed in LS-DYNA. The methodology utilized the marionette method (see section 3.1.1.2)

3.1.1.1 Global transformation

Prior to limb articulation, the entire VIVA+ 50%ile HBM was oriented into the correct global coordinate system using the transformation (`*DEFINE_TRANSFORMATION`) key.

3.1.1.2 Marionette Method

To reposition the limbs into the walking posture without inducing severe localized mesh distortions, a force-driven cable-pulling mechanism called the Marionette method was implemented. One-dimensional discrete beam elements (`*ELEMENT_BEAM`) were constructed, utilizing a specific cable material formulation (`*MAT_CABLE_DISCRETE_BEAM`). These virtual cables were routed to connect the nodes of previously identified anatomical landmarks on the VIVA+ 50th %ile HBM extremities directly to their corresponding fixed spatial target nodes extracted from the TB024 skeleton model (Figure 3.2). As the cables contracted during the simulation due to the applied force, the arms and legs were pulled into the designated walking configuration, as shown in the overall setup in Figure 3.3.

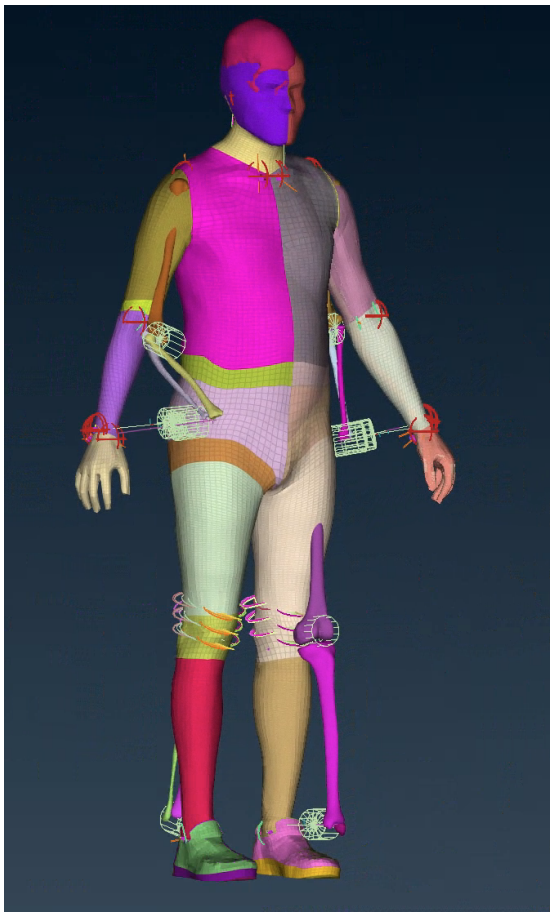

Figure 3.3: The generic TB024 reference skeleton model superimposed onto the VIVA+ 50th %ile HBM to determine target coordinates.

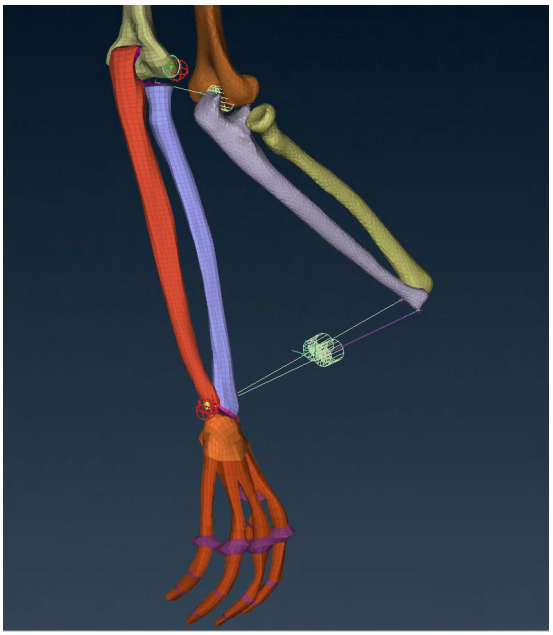

Figure 3.4: Detailed view of the right arm articulation setup, highlighting the cables and viscous dampers.

3.1.1.3 Kinematic Stabilization and Damping

Because repositioning involves the deformation of a highly complex finite element mesh, dynamic stabilization was a requirement to prevent inertial overshoot, unnatural buckling, or high-frequency oscillations. A dual-damping strategy was applied.

- **Localized Viscous Damping:** One-dimensional discrete damper elements (`*ELEMENT_DISCRETE`) with a viscous material model (`*MAT_DAMPER_VISCOUS`) were modeled in parallel with each pulling cable (illustrated in Figure 3.4). A damping coefficient of 0.05 kN $\cdot$ ms/mm was applied to these elements. This specific value was determined iteratively to achieve sufficient resistance to prevent overshoot and high-frequency mesh oscillations. These discrete dampers regulated the velocity of the limbs, ensuring a smooth deceleration as the extremities approached their target coordinates.
- **Global Damping:** A global mass-weighted damping factor of 5% (`*DAMPING_GLOBAL`) was applied to the entire model to continuously dissipate kinetic energy and maintain a quasi-static transition state.

3.1.1.4 Simulation Termination and Validation

The transient positioning simulation was configured to terminate at 300 ms (`*CONTROL_TERMINATION`), providing sufficient time for the VIVA+ 50th %ile HBM to reach a stable, relaxed equilibrium in the new posture, as seen in Figure 3.5.



Figure 3.5: The final walking posture of the VIVA+ 50th %ile HBM achieved after the 300 ms transient simulation.

Upon completion, the final nodal coordinates were extracted, and the resulting joint angles were compared to the Euro NCAP TB024 tolerances. Table 3.1 provides a comparison between the reference and final repositioned angles.

Table 3.1: Validation of the repositioned VIVA+ 50th %ile HBM posture against Euro NCAP TB024 protocol targets.

Abbr.	Measurement	Ref. Value	Tolerance	Actual Value	Deviation
Px	Heel-to-heel distance long.	310 mm	± 5.0%	312.80 mm	+0.90%
Py	Heel to heel distance lateral	185 mm	± 15.0%	184.53 mm	-0.25%
K	Right upper leg angle	89°	±3°	83.25°	−5.75°
L	Left upper leg angle	106°	±5°	100.41°	−5.59°
G	Right knee flexion angle	164°	±3°	169.44°	+5.44°
H	Left knee flexion angle	175°	±5°	174.16°	−0.84°
Ty	Right upper arm angle Y	98°	±3°	96.83°	−1.17°
Uy	Left upper arm angle Y	70°	±3°	72.03°	+2.03°
Tx	Right upper arm angle X	100°	±10°	112.49°	+12.49°
Ux	Left upper arm angle X	100°	±10°	95.20°	−4.80°
V	Right elbow flexion angle	140°	±5°	137.39°	−2.61°
W	Left elbow flexion angle	160°	±10°	151.53°	−8.47°

While the repositioning process aimed to achieve compliance with Euro NCAP TB024, the results indicate that angles K, L, G, and Tx ultimately fell outside the tolerance limits. However it was judged that the model anyway represent the realistic stance.

3.2 HeadForm

In addition to the full-body VIVA+ 50th %ile HBM simulations, a standard headform impactor was used to evaluate head injury across the same parametric matrix of heights of the simplified truck model and impact speeds. The headform represents the conventional test tool used in Euro NCAP pedestrian assessment protocols and serves as a point of comparison against the VIVA+ 50th %ile HBM.

The headform is a spherical impactor with a diameter of 165 mm and a total mass of 4.5 kg, representing the head of a 50th-percentile male adult. The headform consist of a rigid sphere coated with a rubber hull. A triaxial accelerometer is mounted at the centre of gravity of the impactor to measure the resultant head acceleration time history during contact, from which the Head Injury Criterion (HIC15) is calculated in post-processing [18].

The headform simulations utilized the LSTC Pedestrian Headform Adult model developed by Livermore Software Technology Corporation (LSTC). This finite element model is explicitly validated against the ECE/324 and ECE/TRANS/505 regulations [33].

After positioning the 50th %ile VIVA+ HBM in front of the simplified truck model,

the position of the head was noted with respect to the origin point (0,0,0) in the ANSA environment, and the standard impactor headform was positioned accordingly to match the exact location of the head at the time of impact using (`*DEFINE_TRANSFORMATION`) control cards.

3.3 Simplified Truck Model

For the simulation study, a simplified generic truck front end was provided by Volvo. The simplified truck model was not validated. 12 tonnes of mass was added using lumped mass at the rear end of the simplified truck model. A separate key file was used to define all cards for the VIVA+ 50th %ile HBM and simplified truck model (similarly, a separate key file for the headform and simplified truck model) for the simulations.

The simplified truck model includes parts such as: windshield, wiper panel, front lid, radiator assembly, lower front, front chassis frame, and front cabin suspension, however using simplified material definitions.

3.4 Parametric Study and Simulation Setup

Table 3.2 outlines the parametric study carried out. A total of 8 simulations were carried out, including both 40km/h and 24km/h truck speeds for the VIVA+ 50th %ile HBM, by setting the front end height of the simplified truck model to be 120, 220, 320, and 420 mm.

Table 3.2: Detailed parametric simulation matrix.

Truck ground height	120mm		220mm		320mm		420mm	
Speed (in km/h)	24	40	24	40	24	40	24	40
Impactor	VIVA+ 50th %ile HBM							
	Headform							

Figure 3.6 below depicts the variations of the simplified truck model height in front of the VIVA+ 50th %ile HBM. The simplified truck model was defined with the respective initial velocities using (`*INITIAL_VELOCITY_GENERATION`) for the entire model and for the lumped mass in the +X direction.

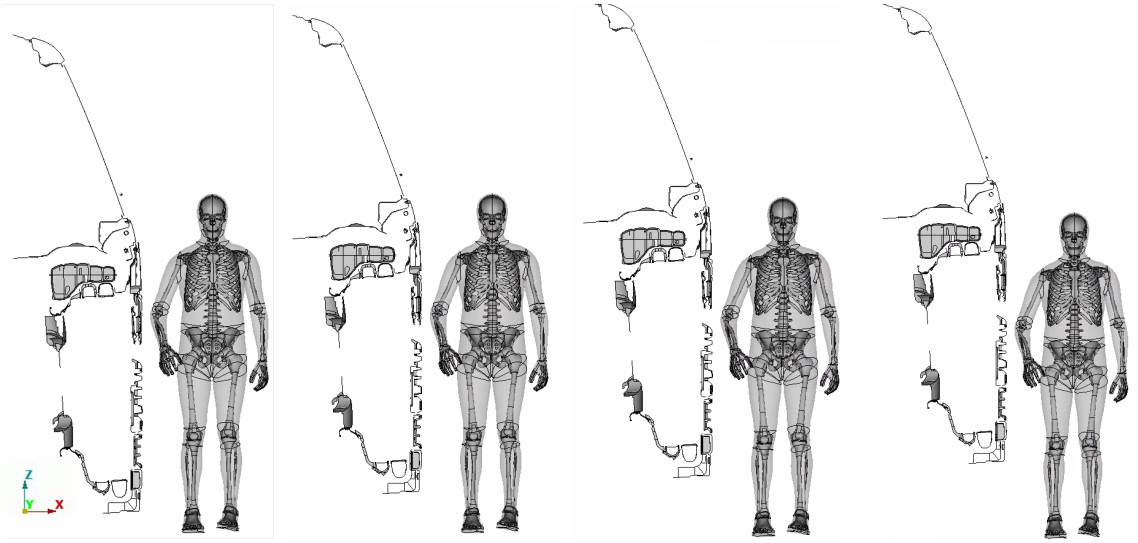

(a) 120mm (b) 220mm (c) 320mm (d) 420mm

Figure 3.6: Comparison of the four parametric ground heights of the simplified truck model in front of the VIVA+ 50th %ile HBM

Similarly, 8 simulations were run in where the headform impacting the simplified truck model at both 40 km/h and 24 km/h for all four truck heights. The impact velocity was defined for the head-form model using (`*INITIAL_VELOCITY_GENERATION`) in the -X direction, while the simplified truck model was constrained to be stationary.
Figure 3.7 depicts the variations of the truck height in front of the headform.

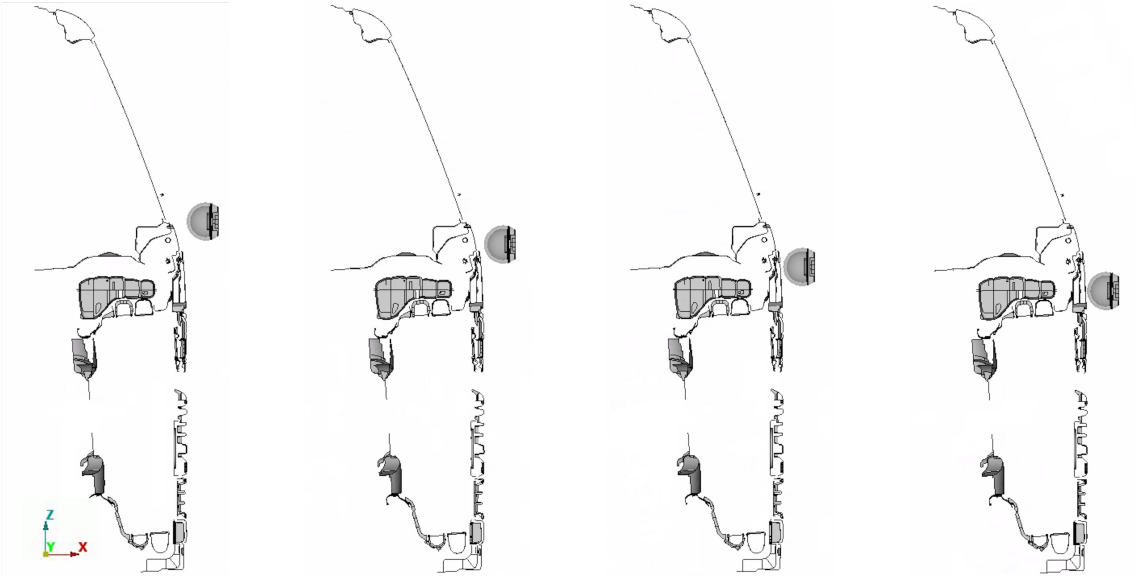

(a) 120mm (b) 220mm (c) 320mm (d) 420mm

Figure 3.7: Comparison of the four ground heights of the simplified truck model in front of the headform.

4
Results

In this chapter, the results of the parametric simulations are presented, detailing the injury outcomes from a simplified truck model impacting the VIVA+ 50th %ile HBM and standard headform impacts on the simplified truck model.

4.1 Crash Kinematics

Figure 4.1 illustrates the crash kinematics of the VIVA+ 50th %ile HBM when it was impacted by the simplified truck model at 40 km/h with 320 mm ground height at the time mentioned in the respective figure caption.

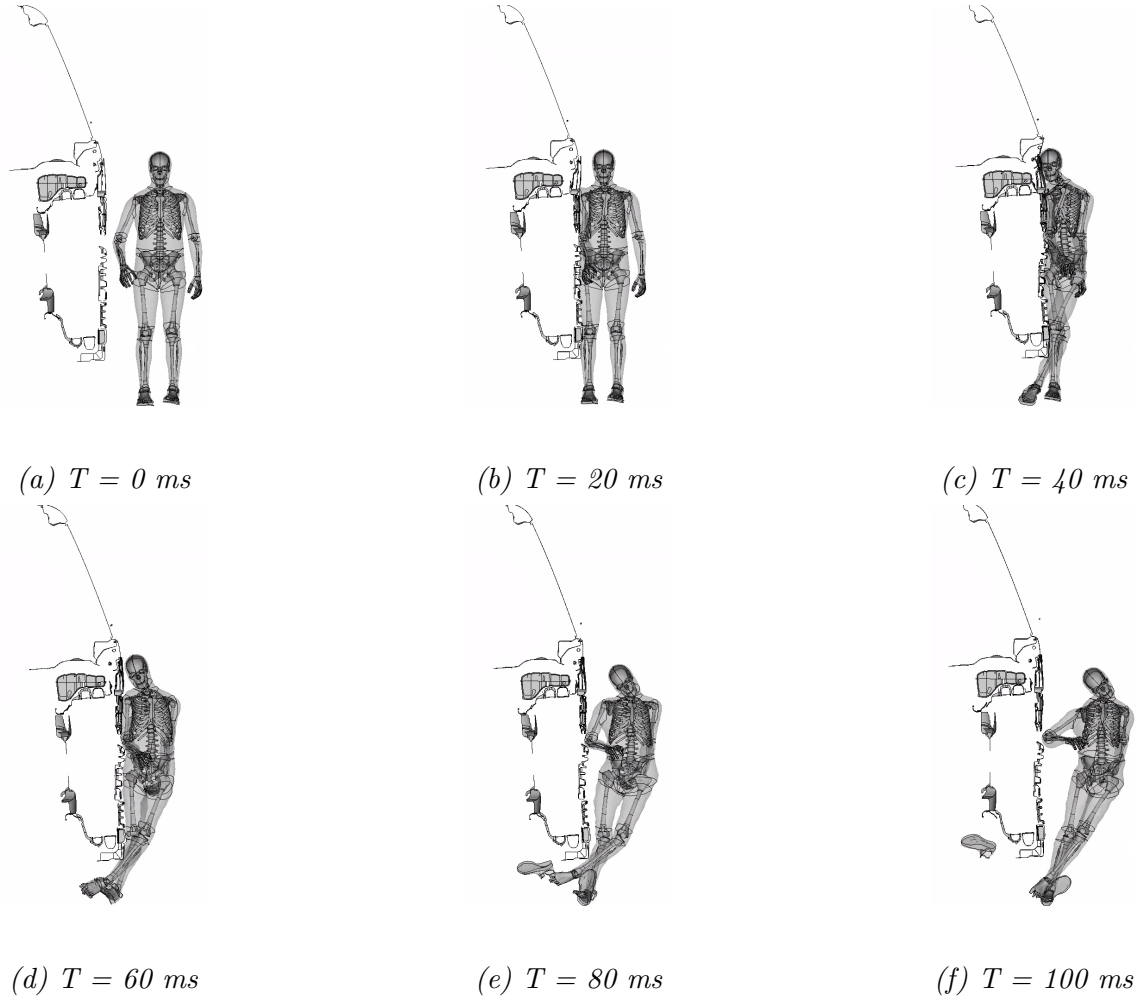

(a) T = 0 ms *(b) T = 20 ms* *(c) T = 40 ms*

(d) T = 60 ms *(e) T = 80 ms* *(f) T = 100 ms*

Figure 4.1: Full Body Crash kinematics of the VIVA+ 50th %ile HBM for 320 mm simplified truck model height at 40 km/h

4.2 Head

Figures A.1 to A.8 in A.1.1 detail the head and neck kinematics of the VIVA+ 50th %ile HBM and the resulting head impact locations for all eight VIVA+ 50th %ile HBM simulations. Each figure captures the exact moment of head contact against the simplified truck model, referenced against the initial and final head positions. The figures show that the simplified truck model's height directly dictates the head impact location on the simplified truck model's front (Figure 4.2). Lower simplified truck model height (120 mm) caused the head to impact near the windshield at the wiper panel, while for the rest of the heights, the head impact location shifted to the front lid (Figure 4.3).

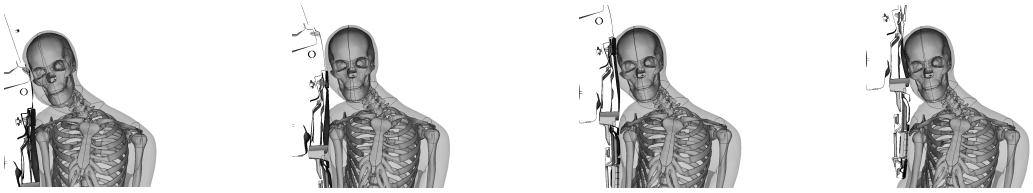

(a) 120 mm *(b) 220 mm* *(c) 320 mm* *(d) 420 mm*

Figure 4.2: Head impact locations of VIVA+ 50th %ile HBM across all the simplified truck model heights



(a) T = 0 ms *(b) T = 25 ms* *(c) T = 30 ms* *(d) T = 50 ms*

Figure 4.3: Close-up head kinematics of the VIVA+ 50th %ile HBM for 120 mm simplified truck model height at 40 km/h

Figures A.9 to A.16 in appendix A.1.1 detail the headform kinematics for both the speeds and the resulting impact location across the four simplified truck model heights referenced against initial and final headform positions. Similar to the VIVA+ 50th %ile HBM's head, the headform's kinematics are dictated by the impact location on the simplified truck model's front. The headform experiences higher rotational displacement at the lower (120 mm) simplified truck model height (refer to figure 4.4) as compared to the rest of the simplified truck model heights, and also higher rotational displacement than VIVA+ 50th %ile HBM.

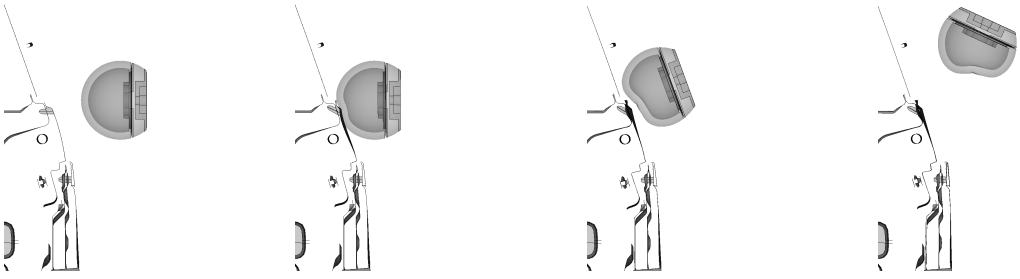

(a) T = 0 ms *(b) T = 7 ms* *(c) T = 20 ms* *(d) T = 50 ms*

Figure 4.4: Close-up kinematics of the headform impact for 120 mm simplified truck model height at 40 km/h.

After carrying out all 16 simulations (8 with VIVA+ 50th %ile HBM and 8 with headform), HIC and DAMAGE for all the simulations were extracted from the

META during post-processing. The following tables 4.1 and 4.2 summarize the results.

Table 4.1: AIS 2+ injury risks for HIC and DAMAGE using equations 2.2 and 2.3 across all four simplified truck model ground heights at 40 km/h and 24 km/h for **VIVA+ 50% ile HBM.**

	40 km/h				24 km/h			
Truck Height	**HIC**	**AIS 2+ Risk**	**DAMAGE**	**AIS 2+ Risk**	**HIC**	**AIS 2+ Risk**	**DAMAGE**	**AIS 2+ Risk**
120	2886	0.88	0.60	0.93	844	0.39	0.36	0.32
220	2036	0.78	0.29	0.16	373	0.11	0.37	0.36
320	1138	0.53	0.24	0.08	271	0.05	0.27	0.13
420	1490	0.65	0.24	0.09	343	0.09	0.27	0.14

Table 4.2: AIS 2+ injury risks for HIC using equation 2.2 across varying simplified truck model ground heights at 40 km/h and 24 km/h for **headform.**

	40 km/h		24 km/h	
Truck Height	**HIC**	**AIS 2+ Risk**	**HIC**	**AIS 2+ Risk**
120	4622	0.95	1046	0.490
220	1654	0.70	351	0.096
320	830	0.38	236	0.038
420	1102	0.51	289	0.063

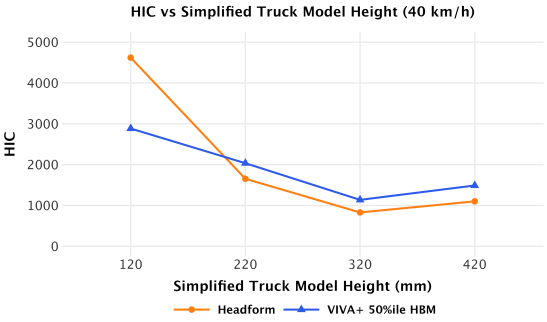

(a) HIC vs simplified truck model height for 40 km/h

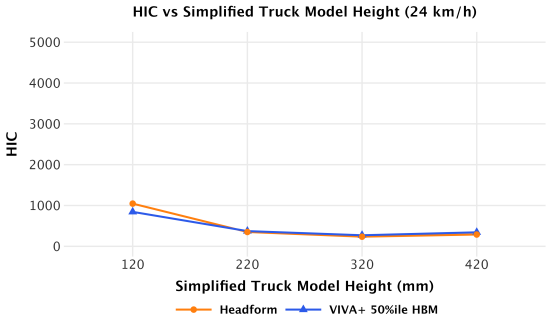

(b) HIC vs simplified truck model height for 24 km/h

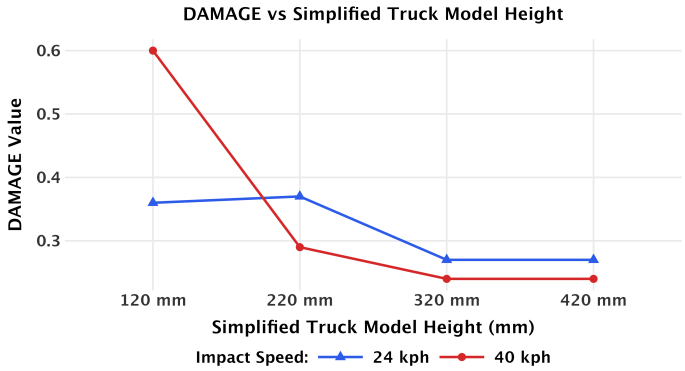

(c) DAMAGE vs simplified truck model heights

Figure 4.5: HIC and DAMAGE across all four simplified truck model heights at 40 km/h and 24 km/h.

The 40 km/h subset of simulations resulted consistently in higher HIC and DAMAGE values than the 24 km/h subset, resulting in higher head and brain injury risks. This trend remained consistent across all simplified truck model heights for both the VIVA+ 50th %ile HBM and the headform (Figure 4.5). Across all simplified truck model heights, the 320 mm resulted in the lowest HIC and DAMAGE values for 24 km/h and 40 km/h, whereas the 120 mm resulted in the highest overall values.

In Figure 4.6 a & b, a comparison of AIS 2+ head injury risk and brain risk is presented for both speeds, and in Figure 4.6 c, AIS 2+ head injury risk for the headform among both speeds is presented. When comparing, the headform generally recorded slightly lower HIC values, resulting in lower head injury risks than the VIVA+ 50% ile HBM (refer to figure 4.5).

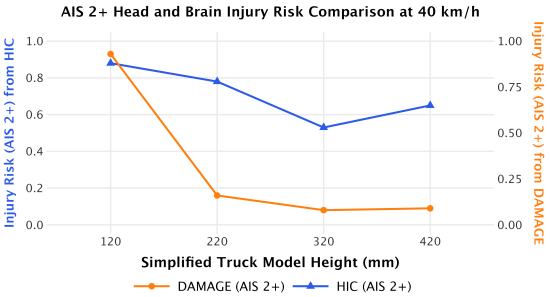

(a) Comparison of Injury risk for Head and Brain for 40 km/h

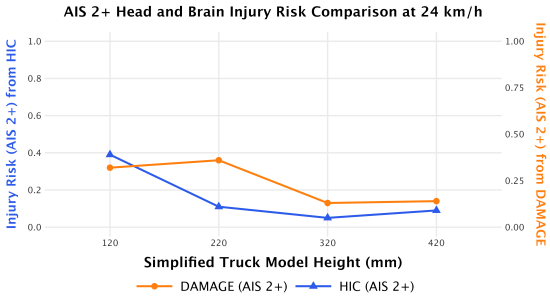

(b) Comparison of Injury risk for Head and Brain for 24 km/h

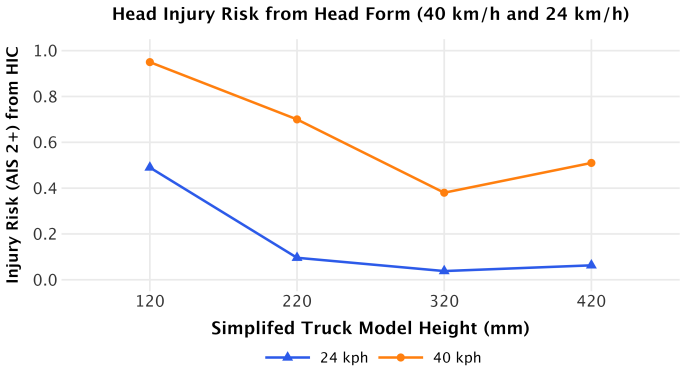

(c) Head Injury Risk (24 km/h and 40 km/h)

Figure 4.6: Comparison of Head and Brain Injury Risks from VIVA+50th %ile HBM and Head Injury Risk for headform

The notable exception occurred at the 120 mm height, where the headform values were higher than the VIVA+ 50% ile HBM results at both impact speeds. This is supported by the compilation of the resultant acceleration curves to plot the Head Injury Criteria for the simplified truck model to VIVA+ 50th %ile HBM and headform crash (refer to figures A.17 and A.18 in appendix A.1.1). In all the resultant acceleration plots for both speeds, the 120 mm simplified truck height resultant acceleration comparatively peaks the highest.

Furthermore, the relationship between simplified truck model ground height and injury risk is observed to be non-linear. The injury metrics exhibit a characteristic 'U-shaped' distribution (refer to figure 4.6); values decrease as the simplified truck model height increases from 120 mm up to 320 mm, but there is an increase in both HIC and DAMAGE values at the 420 mm ground height. Another notable exception is that higher brain injury risk was observed for 24 km/h than for 40 km/h, at 120 mm simplified truck model height.

4.3 Neck

Following the analysis of head injury metrics, this section presents the results of the cervical spine's internal mechanical response during the impact. Figure A.20 in appendix A.2.1 illustrates the neck forces through complete cervical levels (C1-C7). Figure A.21 in appendix A.2.2 illustrates the moments. Force and Moment plots show distinct trends for the two impact speeds. At 40 km/h, the 120 mm simplified truck model height produces noticeably higher neck forces (C1 to C7) compared to the other heights. However, at 24 km/h, the neck forces and moments remain relatively constant across all heights.

4.3.1 Force

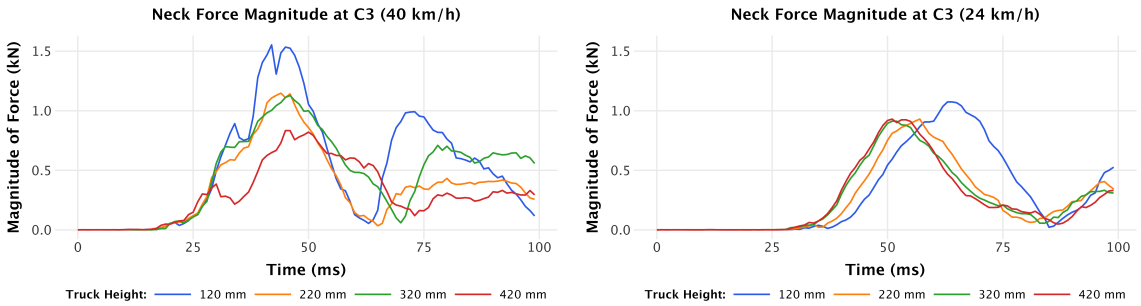

(a) C3 Force at 40 km/h

(b) C3 Force at 24 km/h

Figure 4.7: Comparison of Neck Force (kN) magnitudes at the C3 cross-sections across 40 km/h and 24 km/h impact speeds.

For the 40 km/h crash simulations at a 120 mm truck height, a single force peak occurs near 40 ms in the upper cervical region (C1–C2). The mid-to-lower cervical spine (C3–C7) experiences multiple force peaks, and a maximum force at C3 (refer to Figure 4.7.

At 24 km/h, the multiple peaks are not visible for 120 mm; instead, all four heights produce a singular, clustered peak around 50 ms, except for the 120 mm simplified truck model height, which peaks around 60 ms (Figures A.20 (b and d) in appendix A.2.1). At the mid-cervical (C3-C4), there is a clear, distinct multiple-peak curve at 40 km/h, with the 120 mm curve having the highest magnitude among them all, whereas at 24 km/h, there is a similar pattern to the C1 and C2 plots, the 120 mm curve having a delayed peak compared to the rest of the curves. At the lower cervical (C5-C7), there are the same distinct multiple-peak curves at 40 km/h, with C6 forces being the highest in magnitude, and clustered single-peak curves at 24 km/h.

4.3.2 Moment

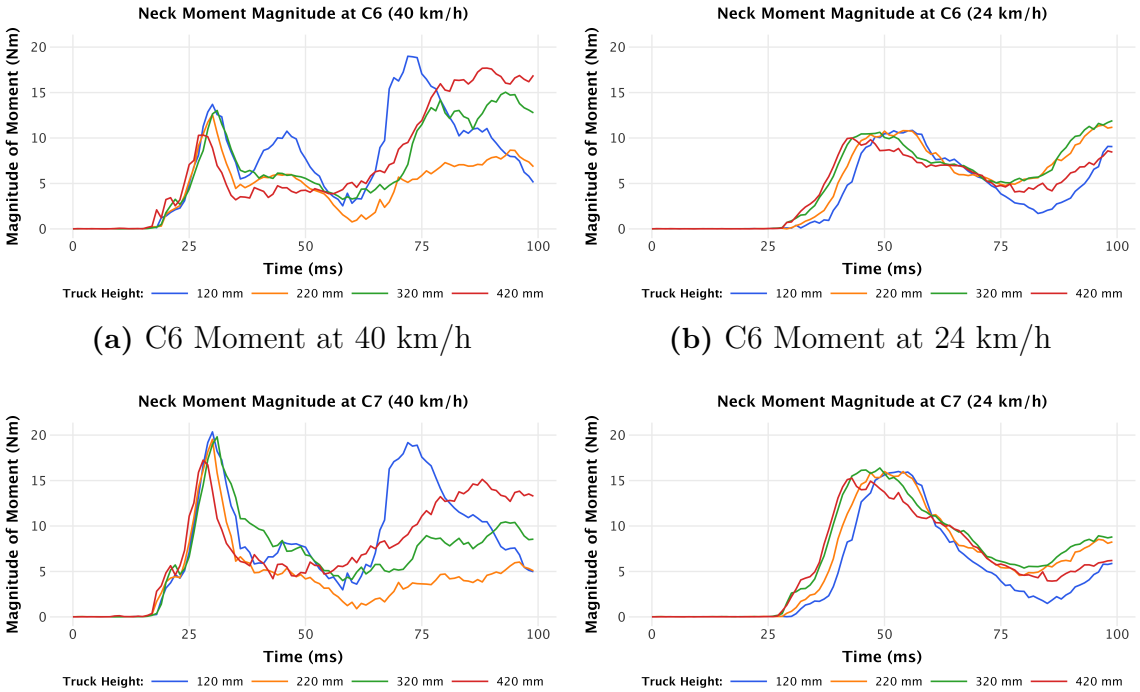

(a) C6 Moment at 40 km/h

(b) C6 Moment at 24 km/h

(c) C7 Moment at 40 km/h

(d) C7 Moment at 24 km/h

Figure 4.8: Neck Moment (Nm) magnitudes at the C6 and C7 cross-sections across 40 km/h and 24 km/h.

In the upper cervical (C1-C2), all four simplified truck model heights produced early moment peaks around 25-30 ms, with 120 mm simplified truck model height curves peaking multiple times at 40 km/h and curves clustered with single peaks around 50 ms at 24 km/h. From the mid-cervical (C3-C4) to the lower cervical (C5-C7 (refer figures 4.8)), there is a different pattern. From C3 downward, the moment plots show a difference from the upper cervical levels; the moments do not peak and then decay; instead, they rise continuously throughout the simulation from around 50 ms all the way to 100 ms, and they are still rising at the end of the simulation. At 24 km/h for (C3–C7), the same rising pattern is present but with lower magnitudes, and again 320 mm and 420 mm tend to produce higher moments than 120 mm, though the differences are lesser. Table 4.3 presents the peak N_{ij} evaluations and the corresponding AIS 3+ neck injury risk for the mid and lower cervical spine.

Table 4.3: Peak N_{ij} Values and AIS 3+ Injury Risk for Mid and Lower Cervical Levels at 24 km/h and 40 km/h

Speed	**Level**	**120 mm**		**220 mm**		**320 mm**		**420 mm**	
		N_{ij}	**Risk**	N_{ij}	**Risk**	N_{ij}	**Risk**	N_{ij}	**Risk**
24 km/h	C3	0.301	3.7%	0.284	3.6%	0.279	3.6%	0.292	3.7%
24 km/h	C6	0.274	3.5%	0.286	3.6%	0.275	3.5%	0.267	3.5%
24 km/h	C7	0.298	3.7%	0.313	3.8%	0.314	3.8%	0.303	3.8%
40 km/h	C3	0.473	5.3%	0.352	4.2%	0.347	4.1%	0.262	3.4%
40 km/h	C6	0.412	4.7%	0.272	3.5%	0.270	3.5%	0.243	3.3%
40 km/h	C7	0.403	4.6%	0.298	3.7%	0.302	3.7%	0.263	3.5%

To quantify the injury risk to the cervical spine, the peak resultant neck forces and moments extracted from the simulations were compared against standard Injury Assessment Reference Values (IARVs). Across all evaluated simplified truck model heights and impact speeds, the maximum resultant neck force recorded was approximately 1.5 kN, and the peak bending moment did not exceed 20 Nm. which corresponds to, at 40 km/h, the maximum recorded N_{ij} reaches only 0.473 at the C3 level (during the 120 mm simplified truck model height impact), translating to a maximum AIS 3+ injury risk of 5.3%.

When compared to the established independent tolerance limits for a 50th percentile male, as outlined in Table 2.2 (3600 N for axial tension/compression and 125 Nm for bending), the loads experienced by the VIVA+ 50 %ile HBM fall below the injury thresholds. Hence, the resulting N_{ij} remain below the 1.0 performance limit associated with a 15% risk of an AIS 3+ injury. Therefore, the cervical spine (C1–C7) is predicted to be below AIS3+ injury risk under these specific impact conditions.

4.4 Thorax

The probability of rib fractures was evaluated using the results generation tool within the META post-processing environment, based on calculated maximum strain values for each rib. The resulting fracture risks are presented in Figure 4.9 a and b for 40 km/h and 24 km/h, respectively, using distribution graphs to facilitate comparative analysis across all simplified truck model ground heights and impact velocities.

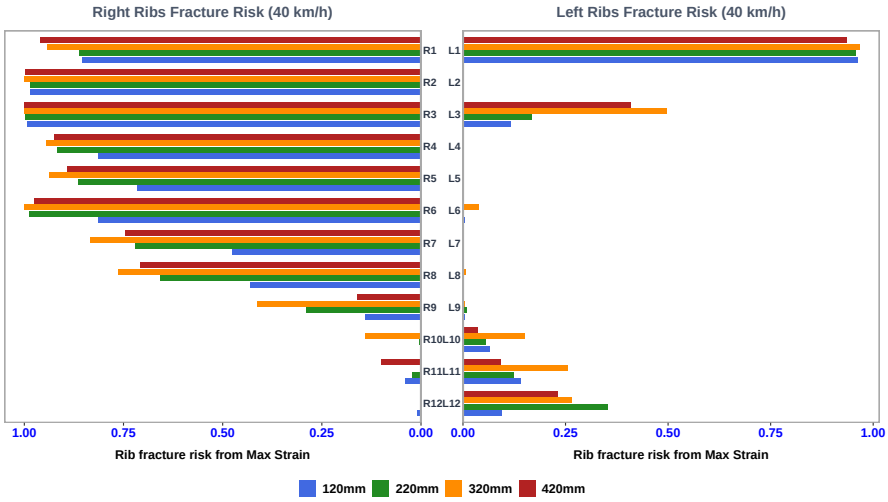

(a) Rib Fracture risk 40 km/h

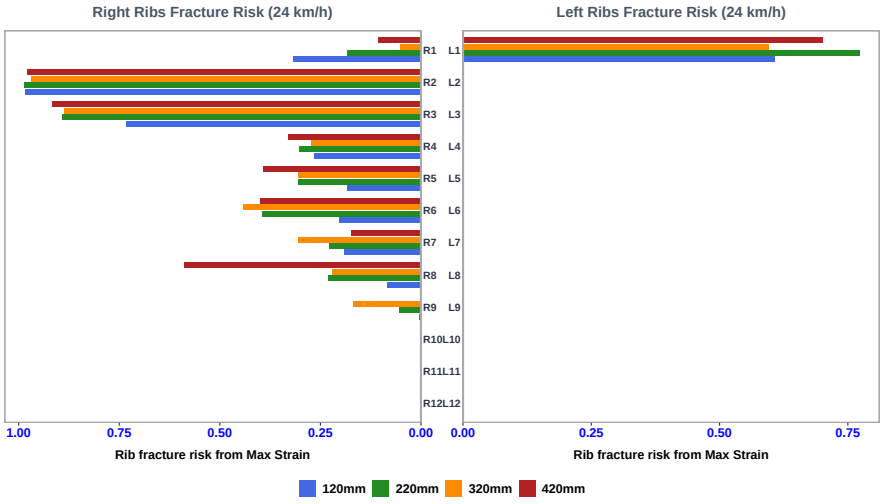

(b) Rib Fracture risk 24 km/h

Figure 4.9: Distribution graphs comparing the rib fracture risks across all simplified truck model ground heights for the 40 km/h and 24 km/h impact scenarios.

During the 24 km/h impact scenarios, ribs R2 and R3 and L1 demonstrated the highest fracture risk across all simplified truck heights. Analysis of the 420 mm sim-

plified truck model height revealed overall higher fracture risks for ribs on the struck side compared to other configurations, with rib R8 demonstrating a substantially higher fracture probability. At a 40 km/h, ribs from R1 to R6 show high fracture risk for all the simplified truck model heights, with less differentiation among heights. Ribs from R7 to R9 also show substantial risk for the 320 mm simplified truck model height in particular. The rib L1 on the non-struck side also exhibited a higher fracture risk for both speeds.

In Figure 4.10, the total number of rib fracture probabilities is shown. At 40 km/h (Figure 4.10a), all four simplified truck height curves start at 100% probability for 2+ fractured ribs. They begin to diverge around the 5+ fractured ribs threshold, depicting at least 5 ribs to be fractured. The 120 mm curve drops most steeply and reaches near zero by 9 or more fractured ribs. The 220 mm, 320 mm, and 420 mm curves stay elevated longer; 320 mm and 420 mm curves maintain probability above 80% all the way to 7+ fractures and do not approach zero even at 10+ ribs.

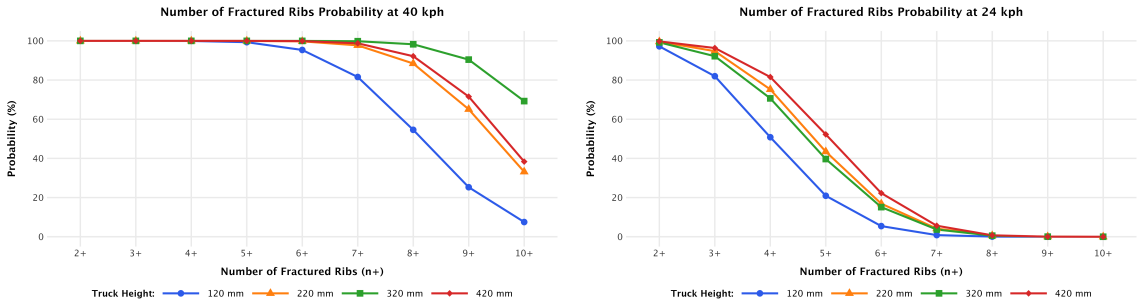

(a) Number of fractured ribs probability for 40 km/h

(b) Number of fractured ribs probability for 24 km/h

Figure 4.10: Total number of fractured ribs probability across all the simplified truck model ground heights at 40 km/h and 24 km/h for 25 YO.

At 24 km/h (Figure 4.10b), the curves separate earlier. The 120 mm curve drops very steeply, falling to near 20% risk of 5+ fractured ribs and reaching zero around 7+ fractured ribs. The 220, 320, and 420 mm curves again stay elevated longer, implying that increased heights correspond to higher injury risk and all reach near zero by 9+ fractured ribs.

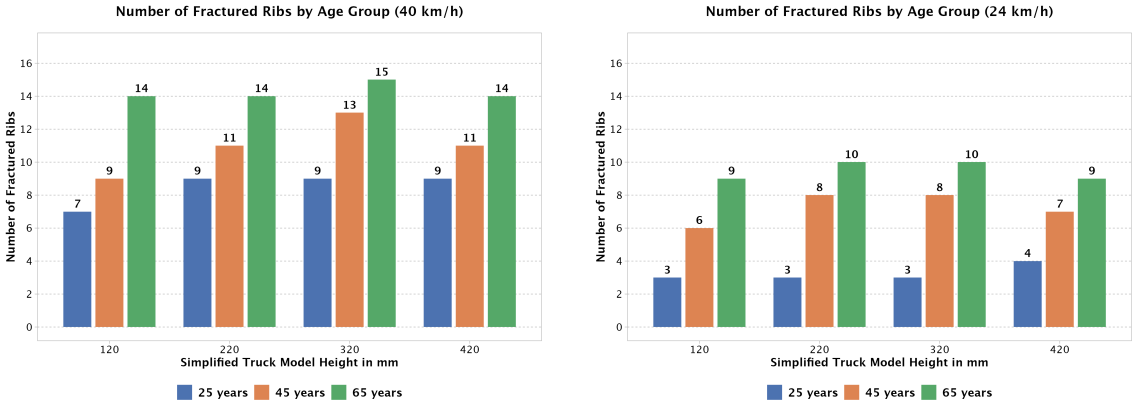

(a) 40 km/h impact speed

(b) 24 km/h impact speed

Figure 4.11: Number of fractured ribs by age group across varying simplified truck model heights for 40 km/h and 24 km/h impact speeds.

In Figure 4.11, the distribution of the number of ribs fractured is shown for 3 different age groups: 25, 45, and 65 Years Old (YO). At 40 km/h, for all four simplified truck model heights, the 25 YO sustains 7–9 fractured ribs, the 45-year-old sustains 9–13 fractured ribs, and the 65 YO sustains 14–15 fractured ribs. The 320 mm height produces the maximum fracture count for both the 45 YO and 65 YO, 13 and 15 ribs, respectively. The 120 mm height produces the lowest counts across all age groups at 40 km/h, with the 25 YO at 7 ribs and the 65 YO at 14. The difference between heights is most pronounced for the 45 YO group, where 320 mm produces 13 versus 120 mm's 9. At 24 km/h, fractured ribs are comparatively lower. The 25-year-old sustains 3–4 fractured ribs across all heights. The 45-year-old ranges from 6 to 8, and the 65-year-old ranges from 9 to 10.

4.5 Lower Extremities

Table 4.4 compiles all the PS99 (99% ile) fracture risks obtained from PS99 strain values extracted from the META-prepost results tool.

Table 4.4: Fracture risks from 99% Strain for the Femur Shaft and Tibia across varying simplified truck model ground heights at 24 km/h and 40 km/h (Left is the Non-struck side, and Right is the Struck side)

	Non-struck side Femur		Struck side Femur		Non-struck side Tibia		Struck side Tibia	
Truck Height	**24 km/h**	**40 km/h**	**24 km/h**	**40 km/h**	**24 km/h**	**40 km/h**	**24 km/h**	**40 km/h**
120	0.005	0.007	0.008	0.015	0.001	0.002	0.001	0.003
220	0.005	0.005	0.004	0.021	0.001	0.005	0.002	0.03
320	0.006	0.04	0.008	0.005	0.001	0.006	0.001	0.1
420	0.004	0.007	0.02	0.32	0	0.017	0.002	0.551

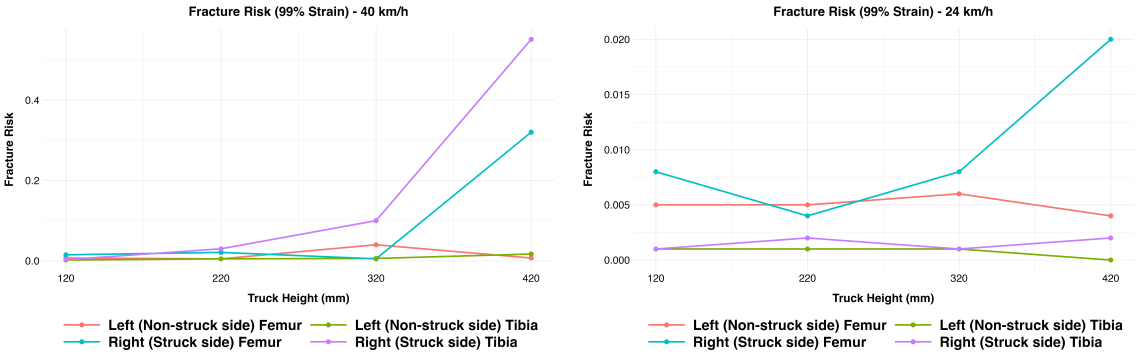

(a) Fracture risk at 40 km/h

(b) Fracture risk at 24 km/h

Figure 4.12: Comparison of 99% Strain fracture risks for the Femur and Tibia across different simplified truck model ground heights.

At 24km/h, refer to Figure 4.12b; neither the Tibia nor the Femur has any notable fracture risk on either side. However, at 40 km/h speed (refer to Figure 4.12a), there is notable fracture risk (more than 30% risk) at 420 mm simplified truck model height for both tibia and femur on the struck side.

5
Discussion

5.1 Head and Brain Injury

5.1.1 Effect of Simplified Truck Model Height and Impact Speed

Head injury risks change noticeably with simplified truck model height and speed. The HIC results follow a non-linear, U-shaped distribution with simplified truck model height at both impact speeds. The 120 mm simplified truck model height produces the highest HIC and DAMAGE values, and 320 mm the lowest. This pattern resulted from the head impact location on the truck front, which is governed by the simplified truck model height.

At 120 mm, the pedestrian's head contacts the wiper panel region of the truck front (Figures A.9 and A.10). The wiper panel is a sloped surface with a higher geometric stiffness than that of the front lid upon which the head is impacted at the rest of the simplified truck model heights. Head impacting at the slope results in combined translational acceleration and rotational velocity, which implies higher HIC and DAMAGE values. The 320 mm height produces the minimum HIC across both speeds, suggesting that this height aligns the head contact with the region of lowest effective stiffness on the truck front.

The 40 km/h simulations consistently produce higher HIC values than the 24 km/h simulations across all truck heights, resulting from higher kinetic energy at the moment of contact and therefore higher peak acceleration (Figure A.17 and Figure A.18 in the appendix A.1.3 detail the compilation of resultant head accelerations). The reduction in HIC between the two speeds is substantial across all heights, confirming that impact speed is a primary determinant of head injury risk.

At 40 km/h, DAMAGE follows the same U-shaped distribution as HIC across the four heights, with 120 mm producing the highest brain injury risk (0.93) and 320 mm the lowest (0.08). This is consistent with the earlier explanation about the wiper panel geometry; the sloped surface generates both translational acceleration (captured by HIC) and rotational velocity (refer to figure A.19) to the head (captured by DAMAGE).

However, a notable exception occurs at 24 km/h: for the 120 mm simplified truck

model height, all the 3 heights produce higher DAMAGE values than those at 40 km/h, which is the opposite of what HIC shows. This inversion between HIC and DAMAGE at 24 km/h needs to be studied further in detail.

5.1.2 Comparison Between VIVA+ 50%ile HBM and Headform Impactor

The headform and VIVA+ 50% ile HBM show similar trends across simplified truck model heights: both produce the highest HIC at 120 mm, the lowest at 320 mm (Figure 4.5).

At 120 mm, the headform produces higher HIC values than the VIVA+ 50% ile HBM at 40 km/h, but similar HIC values at 24 km/h for all the simplified truck model heights. The VIVA+ 50% ile HBM has the head coupled to an articulated cervical spine and torso, whereas the headform is an isolated, unconstrained component. At 40 km/h, the mechanical connection of the neck in the VIVA+ 50% ile HBM differs from the head's overall kinematics compared to the headform, resulting in a lower HIC. However, at the reduced impact speed of 24 km/h, this difference does not lead to a notable divergence in the HIC values. Comparing the headform impact in Figure A.10 with the VIVA+ 50%ile HBM impact in Figure A.2 demonstrates how the presence of the neck and torso visually changes the impact dynamics. Because specific load transfers and forces were not quantified in this study, further detailed analysis is required to determine the exact mechanical factors driving these speed-dependent differences.

Crucially, this comparison highlights that the overall head injury risks predicted by HIC and the DAMAGE metric are not fully correlated. This is due to the distinct injury mechanisms each metric evaluates. HIC is derived primarily from linear acceleration and is correlated with head trauma, such as skull fractures. In contrast, the DAMAGE metric evaluated within the HBM, measures internal brain tissue strain, which is driven by rotational kinematics and correlates with brain trauma. While the unconstrained headform effectively captures the linear acceleration of an impact, it lacks the biofidelity required to replicate the full-body kinematics observed in HBM impacts. Hence, relying solely on HIC from headform testing is insufficient for capturing the overall brain injury risk in heavy goods vehicle collisions. Full-body HBM simulations are essential, as they account for both the linear impacts of the skull and the rotational strains in the brain.

5.2 Neck

The neck force and moment data provide further context for these head injury trends. The higher forces and moments, as observed in the multiple higher peaks of DAMAGE in the simplified truck model at a height of 120 mm, further justify the

significance of the head impact location on the simplified truck model.

The neck is the mechanical link between the head and the rest of the body; its entire loading is dependent upon what the head does during the impact. The multiple peaks observed at the 120 mm simplified truck model height are mainly due to the head kinematics at the sloped wiper panel impact. When the head is struck at the sloped surface, it does not just compress and rebound, rather the slope causes change in the angle of rebound of the head inducing rotational velocity to the head, this contact force has a tangential component that causes the head to partially translate along the slope and then redirect, producing two distinct mechanical events within the same impact sequence leading to multiple peak forces through the cervical spine which is evident the force and moment plots, refer to figures A.20 and A.21. At 24 km/h, the multiple peaks in the force plot disappear because the head of the VIVA+ 50th %ile HBM impacts the wiper panel with lower kinetic energy due to the lower impact speed.

The pattern of moment rise and peaking late (C3 - C7) is evident after the impact; refer to Figure A.21, mainly in the 220 mm, 320 mm, and 420 mm simplified truck model height at 40 km/h. As the shoulders are the initial point of contact with the simplified truck model surface, the body begins its free flight phase, projecting forward and potentially rotating. During this phase, the head of the VIVA+ 50th %ile HBM is no longer constrained by contact force, which is now a mass at the end of the cervical column, and its weight, combined with the ongoing angular momentum of the body, creates a bending moment at the lower cervical levels. As C3–C7 are lower in the neck, they experience the inertial load of everything above them.

The neck data show two different injury mechanisms depending on the simplified truck model height. At 120 mm and 40 km/h, the injury risk is due to early loading of the mid-cervical spine (C3–C4) in a very short time window (25–50 ms), driven by the head's interaction with the sloped wiper panel, in contrast, at 320 mm and 420 mm, the injury risk is on to the lower cervical spine (C5–C7) from the delayed rise in bending moment.

5.3 Thorax

The most consistent finding across the distribution graphs is that (given: right ribs are the struck side and the left ribs are the non-struck side during the impact), during the 40 km/h impacts, ribs through R1 to R8 and L1 are at higher risk of fracture.

The finding that the 120 mm configuration frequently results in lower fracture counts compared to the 320 mm and 420 mm heights is evident from the distribution plots. This is due to the contact interface at the simplified truck model's front. In lower ground-height scenarios (120 mm), the simplified truck model's primary impact surface engages more with the VIVA+ 50th %ile HBM's lower extremities and pelvis, inducing a pushing forward trajectory that distributes the impact load all over the

body. Conversely, at higher ground heights (320 mm and 420 mm), the flat, vertical interface of the simplified truck model's front-end aligns more directly with the thoracic region. This leads to concentration of impact force directly on the ribcage, causing the elevated fracture probabilities observed across the R1–R8 rib segments.

Furthermore, evaluating the injury risk for older pedestrians is essential because individuals aged 65 and older are heavily represented in real-world crash data which directly aligns with the real-world epidemiological data mentioned previously. As highlighted by Malczyk and Bende [14] and the European Commission [4], pedestrians aged 65 and older account for approximately half of all pedestrian fatalities, reported a mortality rate three to seven times higher than younger demographics, this is due to older adults require less thoracic strain to sustain multiple rib fractures (NFR2+), as demonstrated by the Larsson et al. [27], there is a 12.2% reduction in rib cortical bone failure strain for every decade of aging. Future work should expand this analysis by evaluating age-dependent scalars to the head, brain, neck and lower extremities

5.4 Lower Extremities

At 120 mm and 220 mm simplified truck model height, the impact on pedestrians is primarily by the lower front assembly, which contacts the pedestrian's leg at a height that corresponds roughly to the ankle and lower shin region. During this impact, the leg below the knee or at the knee joint, the leg's primary response is rotation about the hip and knee joints rather than direct shaft bending.

At 24 km/h impact speed, neither the tibia nor femur has notable fracture risks, as the contact force is insufficient to drive the strains to produce significant fracture risks among all the simplified truck model heights. However, at a 420 mm simplified truck model height at 40 km/h impact speed, the simplified truck model's lower front impacts the knee joint, transferring kinetic energy to both the tibia and femur, driving higher strains to both bones.

When the simplified truck model's lower front impacts the pedestrian at 420 mm, it makes contact with the femoral shaft, causing the bone to bend at the point of impact and the distal femur to be driven backwards. As the femur collapses, the knee is forced into lateral bending, and the resulting movement drives shear and bending forces down through the knee joint into the proximal tibia. This explains why the tibial fracture risk exceeds 50% at this height under a 40 km/h impact. At lower simplified truck model heights, where the contact occurs at or below the knee, this is not seen, and the tibia remains largely unloaded.

5.5 Overall Injury Risk

The injury risk patterns observed in the simulations align with real-world epidemiological data. As previously discussed, Feist et al. [16] identified the head as the most injured body region in pedestrian-truck collisions (average AIS 3.1), followed by the abdomen/pelvis (average AIS 2.9) and the thorax (average AIS 2.1). The results of this study are aligned with these findings, demonstrating higher injury risks for both the head and thorax, while yielding comparatively low risk probabilities for the neck and lower extremities across the simulated impact speeds and simplified truck heights.

5.6 Conclusion

This study investigated the influence of four parametric simplified truck model heights (120 mm, 220 mm, 320 mm and 420 mm) and simplified truck model speeds (24 km/h and 40 km/h) on pedestrian injury mechanisms and injury severity during the primary impact phase of simplified truck model-to-pedestrian frontal collisions, using VIVA+ 50th %ile HBM and Euro NCAP standard headform impactor. The following conclusions can be drawn from the results.

5.6.1 Head and Brain Injury:

The simplified truck model height primarily dictates the head impact location, which governs the head kinematics during the collision and the severity of head and brain injury. The lower height (120 mm) results in the head being impacted at the slope surface, which induces rotational acceleration. The 320 mm reference simplified truck model height consistently produced lower head and brain injury risks among both speeds in both VIVA+ 50th %ile HBM and headform test methodologies. The injury risk at 40 km/h is higher than at 24 km/h across all the simplified truck model heights, with a 120 mm simplified truck model height producing the highest head and brain injury risks - 0.88 and 0.93, respectively.

5.6.2 Neck Loading

By the comparative analysis of the maximum force and bending moment from the simulations to the IARVs, the neck is at the lower end of the AIS3+ risk curve.

5.6.3 Rib fractures

In conclusion, the thoracic loading analysis shows that rib fracture risks in truck-to-pedestrian simulations can be driven by the impact force loading position onto the VIVA+50th %ile HBM, dependent on the simplified truck model's height.

The increase in rib fracture counts observed particularly in the 45- and 65-year-olds proves the vulnerability of the old age population (60 + years) statistics seen in the

European Road Safety Observatory report of 2023; refer to Figure 1.1

5.6.4 Lower Extremity fractures

Lower extremity fracture risk depends on both the simplified truck model ground clearance height and the impact speed. At 120 mm and 220 mm, and also for the non-struck side, fracture risk remains negligible at both speeds. Only at 420 mm, 40 km/h simplified truck model height and speed, both tibia and femur experience strain, which gives fracture risks at the struck side.

5.6.5 Overall Conclusion

There is no single simplified truck model height that simultaneously minimises injury risk across all body regions. This trade-off is visually summarized in the full-body injury risk maps for each ground height (Figure 5.2). These color-coded distributions (on a scale of green, yellow, orange, and red, as shown in the colour gradient scale in figure 5.1) clearly illustrate the overall injury severities (Head, and brain are illustrated according to AIS 2+ injury risks, neck is illustrated according to AIS 3+ injury risks, Thorax and Lower extremites are illustrated according to fracture risks) across both evaluated impact speeds. The 320 mm simplified truck model height gives lower head and brain injury risks but higher rib fracture risk at 40 km/h speed. While the lower simplified truck model height, 120 mm, and the 220 mm simplified truck model height give lower tibia and femur fracture risks, it increases the head and brain injury risks.

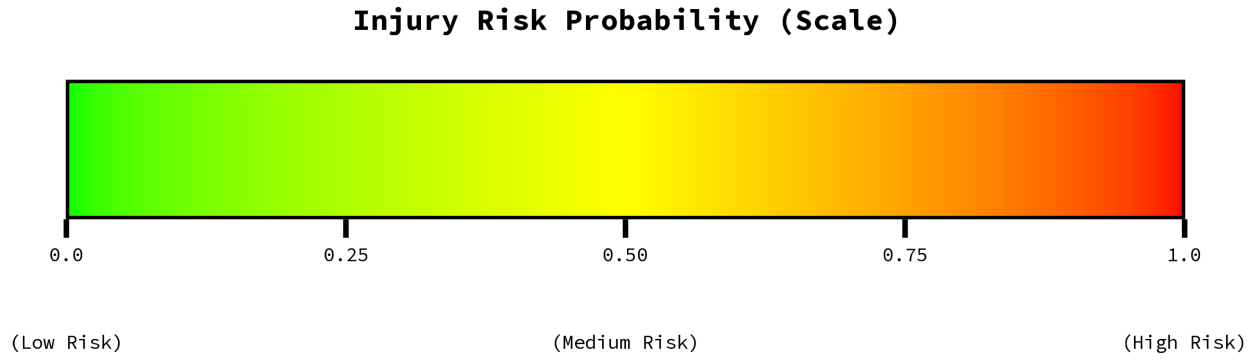

Figure 5.1: Color gradient scale for full-Body injury severity maps ranging from 0.0 (low risk) to 1.0 (high risk).

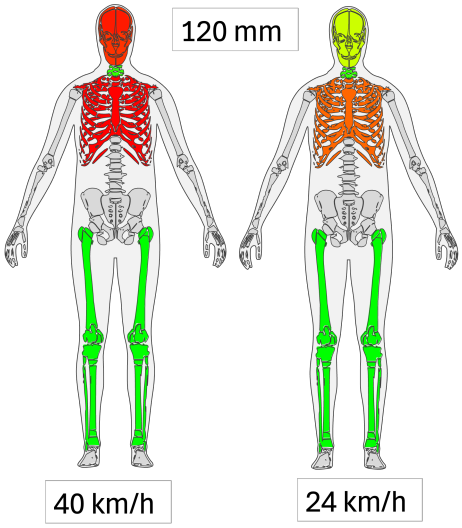

(a) 120 mm Simplified Truck Model Height

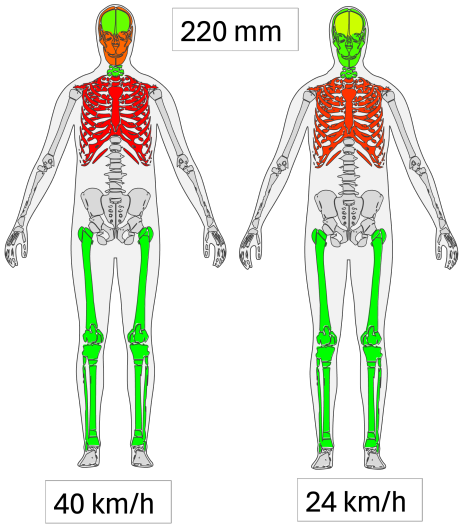

(b) 220 mm Simplified Truck Model Height

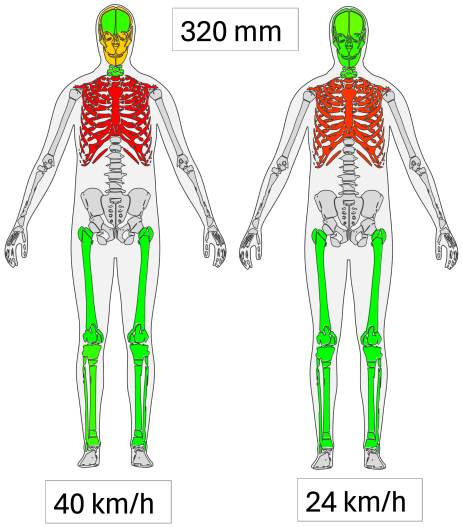

(c) 320 mm Simplified Truck Model Height

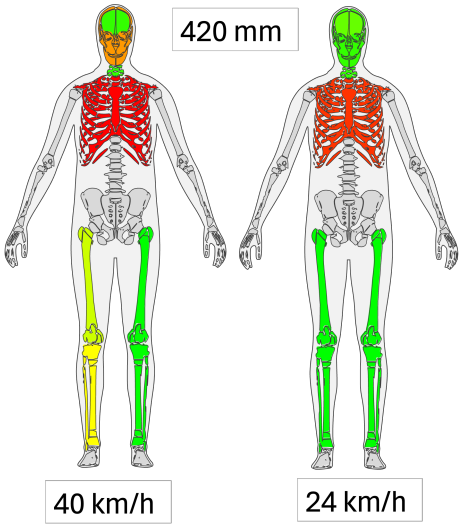

(d) 420 mm Simplified Truck Model Height

Figure 5.2: Full-body injury severity maps illustrating injuries across all four simplified truck model heights at 40 km/h and 24 km/h.

5.7 Future Work

- **Secondary Impact** - This study mainly focused on the primary impact phase between the simplified truck model and the VIVA+ 50% ile HBM. Following the primary impact, the VIVA+ 50% ile HBM is projected forward and undergoes a secondary impact with the ground, which can be a significant contributor to overall injury risk. Future work should extend the current simulations to capture the full impact trajectory and evaluate the complete injury severity.

- **Validated Truck Model** - The truck model currently used was simplified, with generic material models. A future parametric evaluation should be done with a fully validated model with all the material properties for more accurate results.

- **Expanded Pedestrian population** - The current study used only the 50th %ile male VIVA+ HBM in a walking posture. Future work should include a broader range of pedestrian sizes (including both males and females) to understand whether the identified parameters and injury mechanisms generalise across all pedestrian populations.

- **Active safety interaction** - In this study, impact at only two speeds is simulated. Future simulations could include the influence of various active safety system responses, such as automatic emergency braking, to better reflect on real-world scenarios.

5.8 Use of AI

During the preparation of this thesis, generative AI tools were utilised as a supportive resource to assist in the development of data processing scripts to generate graphs using RStudio. An AI-based language tool, Grammarly, was used to assist in proof reading and improving the clarity, grammar, and phrasing of the written text. AI tools such as Gemini and Claude were used as aids in organizing and structuring written content during the drafting process and to help with the drafting in LaTeX code. No AI tool was used to generate, fabricate, or alter any simulation data, results, or figures presented in this thesis (except for the figure 2.1, where Gemini was used to enhance the view of the cervical spine and the labels for clear illustration to readers). The candidate takes full responsibility for the accuracy, integrity, and originality of all the content presented, including any text that was refined with the assistance of AI tools.

Bibliography

[1] Gustaver, M. (2020) A Chalmers University of Technology Master's thesis template for LaTeX. Unpublished.

[2] ITF (2023), ITF Transport Outlook 2023, OECD Publishing, Paris, https://doi.org/10.1787/b6cc9ad5-en.

[3] United Nations Conference on Trade and Development (UNCTAD) / Sustainable Freight Transport Framework. *Key Freight Transport-Related Data*. Available at: sft-framework.unctad.org

[4] European Commission (2021) Facts and Figures Pedestrians. European Road Safety Observatory. Brussels, European Commission, Directorate General for Transport https://road-safety.transport.ec.europa.eu/system/files/2023-02/ff_pedestrians_20230213.pdf

[5] Tomasch, E., & Smit, S. (2023). Naturalistic driving study on the impact of an aftermarket blind spot monitoring system on the driver's behaviour of heavy goods vehicles and buses on reducing conflicts with pedestrians and cyclists Accident Analysis & Prevention, 191, 107242.doi.org, ISSN 0001-4575, https://www.sciencedirect.com/science/article/pii/S0001457523002890

[6] Wen Hu, Samuel S. Monfort, Jessica B. Cicchino, The association between passenger-vehicle front-end profiles and pedestrian injury severity in motor vehicle crashes, Journal of Safety Research, Volume 90, 2024, Pages 115-127, ISSN 0022-4375, https://doi.org/10.1016/j.jsr.2024.06.007. https://www.sciencedirect.com/science/article/pii/S0022437524000859

[7] Monfort, S. S., Hu, W., & Mueller, B. C. (2024). Vehicle front-end geometry and in-depth pedestrian injury outcomes. Traffic Injury Prevention, 25(4), 631–639. https://doi.org/10.1080/15389588.2024.2332513

[8] National Highway Traffic Safety Administration (NHTSA), "Traffic Safety Facts 2023 Data: Pedestrians," U.S. Department of Transportation, Washington, D.C., 2023. [Online]. Available: https://www.nhtsa.gov/road-safety/pedestrian-safety

[9] https://www.who.int/news/item/13-12-2023-despite-notable-progress-road-safety-remains-urgent-global-issue Date accessed - 15 February 2026

[10] https://www.nhtsa.gov/book/countermeasures-that-work/pedestrian-safety Date accessed - 15 February 2026

[11] S.-L. Chong, L.-W. Chiang, J. C. Allen, E. W. Fleegler, and L. K. Lee, "Epidemiology of Pedestrian-Motor Vehicle Fatalities and Injuries, 2006-2015," *American Journal of Preventive Medicine*, vol. 55, no. 1, pp. 98–105, 2018. [Online]. Available: https://doi.org/10.1016/j.amepre.2018.03.023

[12] T. Dukic Willstrand, K. Holmquist, R. Fredriksson, and M. Rizzi, "Potential of heavy goods vehicle countermeasures to reduce the number of fatalities in crashes with vulnerable road users in Sweden," *Traffic Safety Research*, 2024. [Online]. Available: https://doi.org/10.55329/tsr.2024.123

[13] P. Puthan, R. Fredriksson, S. Thorn, and F. Törnvall, "Real World Accident Analysis of Truck Front Impact to Pedestrians," in *Proceedings of the IRCOBI Conference*, Malaga, Spain, 2016. [Online]. Available: http://www.ircobi.org/wordpress/downloads/irc16/pdf-files/104.pdf

[14] A. Malczyk and J. Bende, "Accidents between heavy goods vehicles and vulnerable road users," *German Insurers Accident Research (UDV)*, 2019. [Online]. Available: https://udv.de/en

[15] Y. Matsui, S. Oikawa, K. Sorimachi, A. Imanishi, and T. Fujimura, "Association of Impact Velocity with Risks of Serious Injuries and Fatalities to Pedestrians in Commercial Truck-Pedestrian Accidents," *Stapp Car Crash Journal*, vol. 60, pp. 165–182, 2016. [Online]. Available: https://www.stapp.org/stapp.shtml

[16] F. Feist, J. Gugler, C. Arregui-Dalmases, E. del Pozo de Dios, F. López-Valdés, C. Deck, and R. Willinger, "Pedestrian Collisions with Flat-Fronted Vehicles: Injury Patterns and Importance of Rotational Accelerations as a Predictor for Traumatic Brain Injury (TBI)," in *21st International Technical Conference on the Enhanced Safety of Vehicles (ESV)*, Stuttgart, Germany, 2009. [Online]. Available: https://www-esv.nhtsa.dot.gov/Proceedings/21/files/09-0264.pdf

[17] Y. Han, J. Yang, K. Mizuno, and Y. Matsui, "A study on chest injury mechanism and the effectiveness of a headform impact test for pedestrian chest protection from vehicle collisions," *Safety Science*, vol. 50, no. 2, pp. 1304–1312, 2012. [Online]. Available: https://research.chalmers.se/en/publication/156822

[18] https://dyna.oasys-software.com/content/uploads/2025/04/2022-Headforms.pdf Date accessed: 7 March 2026

[19] SAE International, "SAE J2782: Performance Specifications for a Midsize Male Pedestrian Research Dummy," Surface Vehicle Information Report, Nov. 2019. [Online]. Available: https://www.sae.org/standards/content/j2782_201911/

[20] L. J. Sundblad and P. Wassenius, "The human body model VIVA+ in far-side collisions: A validation and evaluation study of HBM usage," Master's Thesis, Dept. of Mechanics and Maritime Sciences, Chalmers University of Technology, Gothenburg, Sweden, 2022. [Online]. Available: https://odr.chalmers.se

[21] C. Klug, F. Feist, B. Schneider, and M. van Ratingen, "Development of a Certification Procedure for Numerical Pedestrian Models," in *12th European LS-DYNA Conference*, Koblenz, Germany, 2019. [Online]. Available: https://www.researchgate.net/publication/335126817

[22] Euro NCAP, "Technical Bulletin 024: Pedestrian Human Model Certification," Version 3.0.1, European New Car Assessment Programme, Nov. 2021. [Online]. Available: https://www.euroncap.com

[23] Chapter 14 - Human body Models by Karin Brolin Tiwari, G., Mohan, D., & Agrawal, G. (Eds.). (2016). Transport Planning and Traffic Safety: Making Cities, Roads, and Vehicles Safer (1st ed.). CRC Press. https://doi.org/10.1201/b19737

[24] The TB024 Reference skeleton of a pedestrian in walking stance: https://openvt.eu/EuroNCAP/tb024/-/tree/master/03_Reference_Skeleton/LS-Dyna?ref_type=heads Date accessed - 20 February 2026

[25] Development of Improved Injury Criteria for the Assessment of Advanced Automotive Restraint Systems - II. Tannous, Rabih & Eppinger, Rolf & Sun, Emily & Bandak, Faris & Haffner, Mark & Khaewpong, Nopporn & Maltese, Matt & Kuppa, Shashi & Nguyen, Thuvan & Takhounts, Erik & Zhang, Anna & Saul, Roger. (1999).

[26] Title: Supplement: development of improved injury criteria for the assessment of advanced automotive restraint systems: II Creator(s) : Eppinger, Rolf;Kuppa, Sashi;Saul, Roger;Sun, Emily; Published Date: 2000-03-01 https://rosap.ntl.bts.gov/view/dot/14739

[27] Larsson K-J, Blennow A, Iraeus J, Pipkorn B and Lubbe N (2021) Rib Cortical Bone Fracture Risk as a Function of Age and Rib Strain: Updated Injury Prediction Using Finite Element Human Body Models. Front. Bioeng. Biotechnol. 9:677768. doi:10.3389/fbioe.2021.677768

[28] Forman JL, Kent RW, Mroz K, Pipkorn B, Bostrom O, Segui-Gomez M. Predicting rib fracture risk with whole-body finite element models: development and preliminary evaluation of a probabilistic analytical framework. Ann Adv Automot Med. 2012;56:109-24. PMID: 23169122; PMCID: PMC3503420.

[29] Schubert, A., Erlinger, N., Leo, C. et al (2021). Development of a 50th Percentile Female Femur Model. Conference proceedings International Research Council on the Biomechanics of Injury, IRCOBI, 2021-September: 308-332

[30] L. Shi, Y. Han, H. Huang, W. He, F. Wang, and B. Wang, "Effects of vehicle front-end safety countermeasures on pedestrian head injury risk during ground impact," *Proc IMechE Part D: J Automobile Engineering*, vol. 233, no. 14, pp. 3588–3599, 2019. [Online]. Available: https://doi.org/10.1177/0954407019828845

[31] M. C. Hinzmann, "Analysis of impact kinematics in VRU/vehicle collisions using parameterised HBM - FE simulations," Master's Thesis, KTH Royal Institute of Technology, Stockholm, Sweden, 2025. [Online]. Available: https://www.diva-portal.org/smash/get/diva2:2004507/FULLTEXT01.pdf

[32] Euro NCAP, "Technical Bulletin 035: Brain Injury Calculation," Version 1.0.1, European New Car Assessment Programme. [Online]. Available: https://cdn.euroncap.com/cars/assets/tb_035_brain_injury_calculation_v101_c2c66b7d6c.pdf

[33] Livermore Software Technology Corporation. (2018). LSTC Pedestrian Headform Adult Model (Version 1.06 BETA / 180601) [Finite element model].https://lsdyna.ansys.com/lstc-dummy-models-overview/?utm_source=gemini

[34] Schmitt, K.-U., Niederer, P. F., Cronin, D. S., Morrison, B., III, Muser, M. H., & Walz, F. (2019). Trauma biomechanics: An introduction to in-

jury biomechanics (5th ed.). Springer. https://link.springer.com/book/10.1007/978-3-030-11659-0

[35] Criteria for injury potential. In: Impact acceleration stress symposium. National Academy of Sciences, Washington, National Research Council, Pub. No. 977, pp 141–144

[36] Kerrigan, J., Bhalla, K., Madeley, N., Funk, J., et al., "Experiments for Establishing Pedestrian-Impact Lower Limb Injury Criteria," SAE 2003 World Congress & Exhibition, Detroit, Michigan, United States, March 3, 2003, https://doi.org/10.4271/2003-01-0895

[37] Versace J (1971) A review of the severity index. In: Proceedings of the 15th Stapp car crash conference, SAE 710881

[38] Development of a Second-Order System for Rapid Estimation of Maximum Brain Strain. Annals of Biomedical Engineering, Vol. 47, No. 9, September 2019 (Ó 2018) pp. 1971–1981 https://doi.org/10.1007/s10439-018-02179-9. https://link.springer.com/content/pdf/10.1007/s10439-018-02179-9.pdf

[39] Preliminary Sex-specific Relationships between Peak Force and Cortical Bone Morphometrics in Human Tibiae Subjected to Lateral Loading, Proceedings of IRCOBI Conference 2021. https://www.ircobi.org/wordpress/downloads/irc21/pdf-files/2133.pdf

[40] Dynasaur Library, OpenVT Github repository https://openvt.eu/fem/viva/vivaplus-validation/-/tree/main/catalog/Harden-2021-Tibia-shaft?ref_type=heads

A

Appendix

A.1 Head Results

A.1.1 HBM head crash kinematics

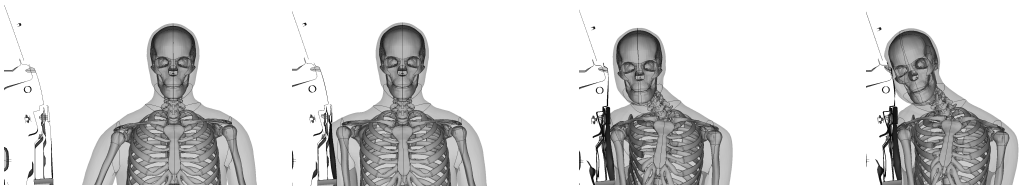

(a) T = 0 ms *(b) T = 25 ms* *(c) T = 50 ms* *(d) T = 60 ms*

Figure A.1: Close-up head kinematics of the VIVA+ 50th %ile HBM for 120 mm simplified truck model height at 24 km/h



(a) T = 0 ms *(b) T = 25 ms* *(c) T = 30 ms* *(d) T = 50 ms*

Figure A.2: Close-up head kinematics of the VIVA+ 50th %ile HBM for 120 mm simplified truck model height at 40 km/h

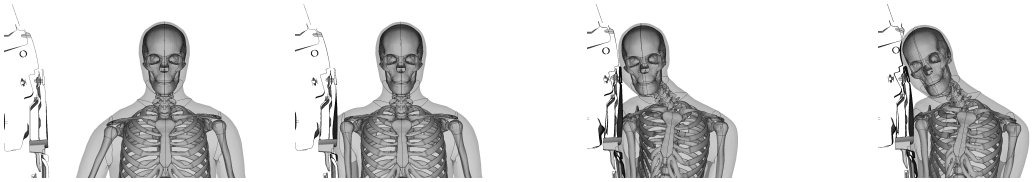

(a) T = 0 ms *(b) T = 25 ms* *(c) T = 50 ms* *(d) T = 60 ms*

Figure A.3: Close-up head kinematics of the VIVA+ 50th %ile HBM for 220 mm simplified truck model height at 24 km/h

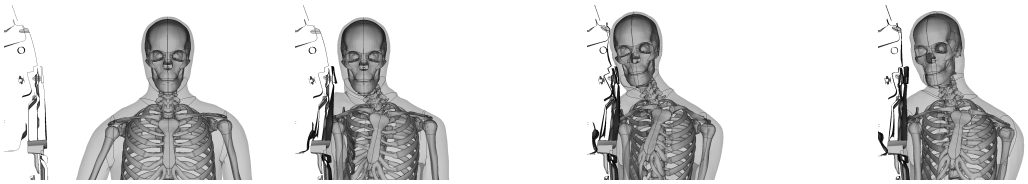

(a) T = 0 ms *(b) T = 25 ms* *(c) T = 40 ms* *(d) T = 50 ms*

Figure A.4: Close-up head kinematics of the VIVA+ 50th %ile HBM for 220 mm simplified truck model height at 40 km/h

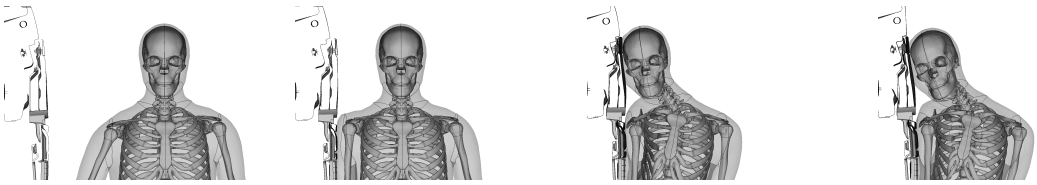

(a) T = 0 ms *(b) T = 25 ms* *(c) T = 50 ms* *(d) T = 60 ms*

Figure A.5: Close-up head kinematics of the VIVA+ 50th %ile HBM for 320 mm simplified truck model height at 24 km/h



(a) T = 0 ms *(b) T = 25 ms* *(c) T = 30 ms* *(d) T = 50 ms*

Figure A.6: Close-up head kinematics of the VIVA+ 50th %ile HBM for 320 mm simplified truck model height at 40 km/h

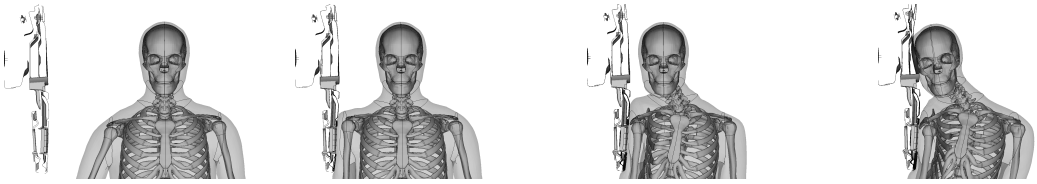

(a) T = 0 ms *(b) T = 25 ms* *(c) T = 40 ms* *(d) T = 50 ms*

Figure A.7: Close-up head kinematics of the VIVA+ 50th %ile HBM for 420 mm simplified truck model height at 24 km/h



(a) T = 0 ms *(b) T = 20 ms* *(c) T = 30 ms* *(d) T = 50 ms*

Figure A.8: Close-up head kinematics of the VIVA+ 50th %ile HBM for 420 mm simplified truck model height at 40 km/h

A.1.2 Headform crash kinematics

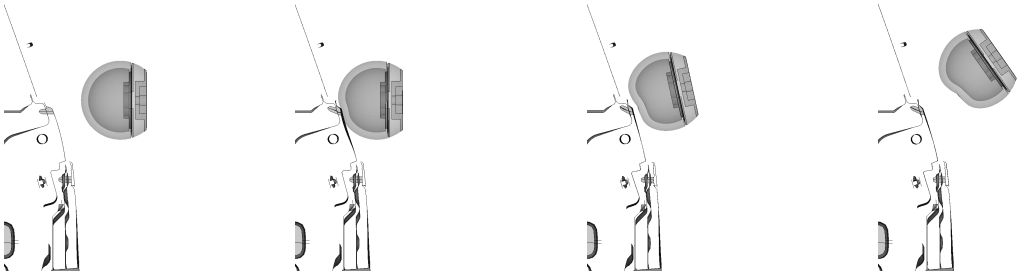

(a) T = 0 ms *(b) T = 10 ms* *(c) T = 25 ms* *(d) T = 50 ms*

Figure A.9: Close-up kinematics of the headform impact for 120 mm simplified truck model height at 24 km/h.

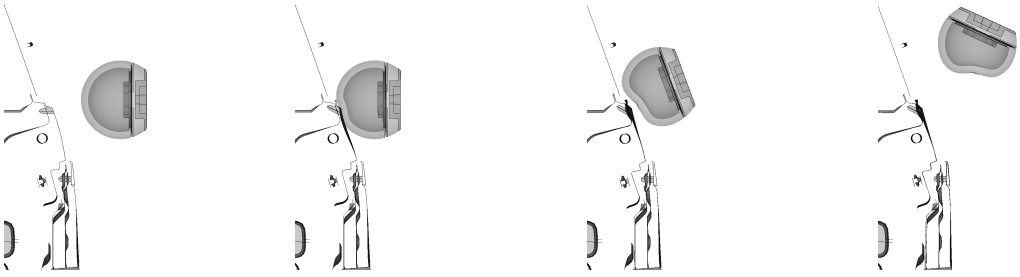

(a) T = 0 ms *(b) T = 7 ms* *(c) T = 20 ms* *(d) T = 50 ms*

Figure A.10: Close-up kinematics of the headform impact for 120 mm simplified truck model height at 40 km/h.

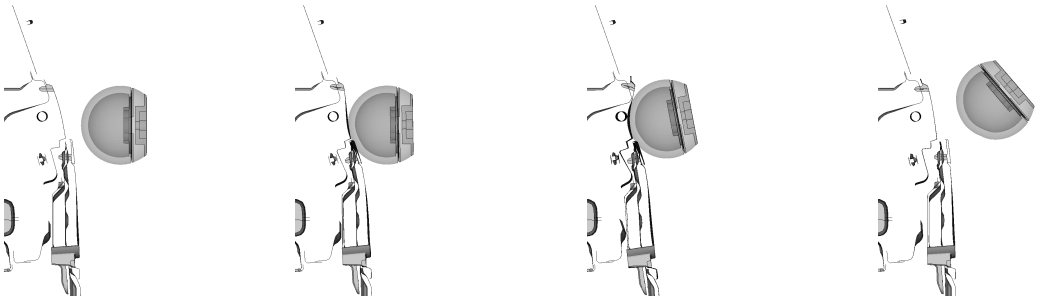

(a) T = 0 ms *(b) T = 8 ms* *(c) T = 20 ms* *(d) T = 50 ms*

Figure A.11: Close-up kinematics of the headform impact for a 220 mm simplified truck model height at 24 km/h.

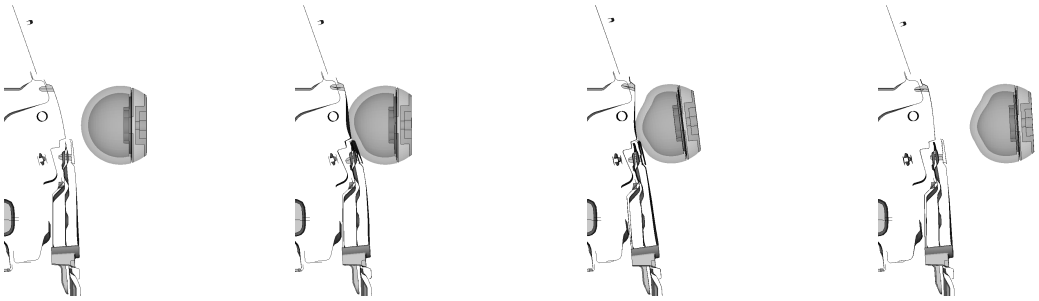

(a) T = 0 ms *(b) T = 5 ms* *(c) T = 25 ms* *(d) T = 50 ms*

Figure A.12: Close-up kinematics of the headform impact for a 220 mm simplified truck model height at 40 km/h.

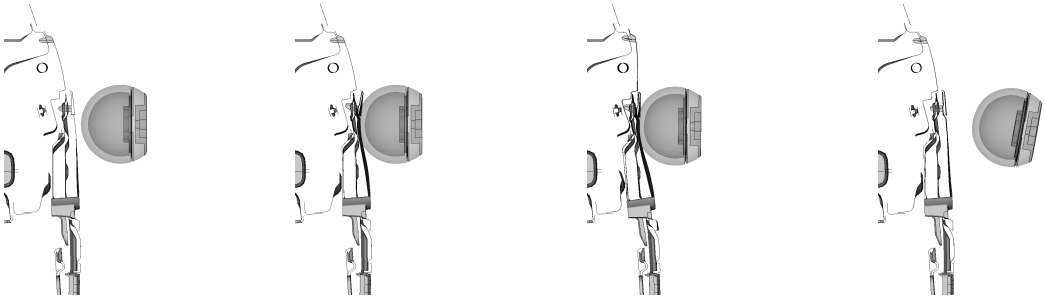

(a) T = 0 ms *(b) T = 5 ms* *(c) T = 20 ms* *(d) T = 50 ms*

Figure A.13: Close-up kinematics of the headform impact for 320 mm simplified truck model height at 24 km/h.

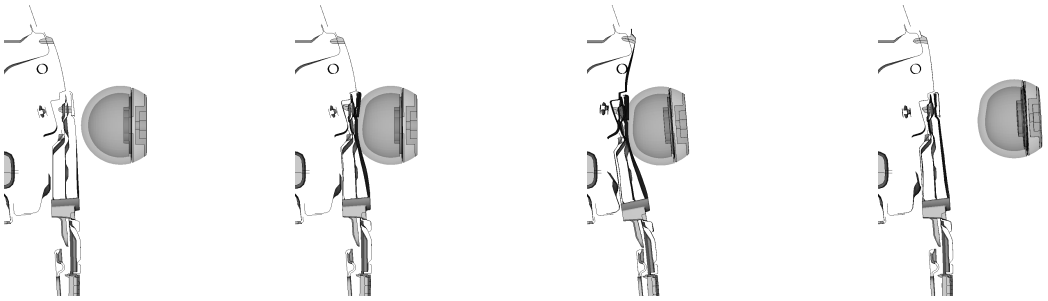

(a) T = 0 ms *(b) T = 4 ms* *(c) T = 15 ms* *(d) T = 50 ms*

Figure A.14: Close-up kinematics of the headform impact for a 320 mm simplified truck model height at 40 km/h.

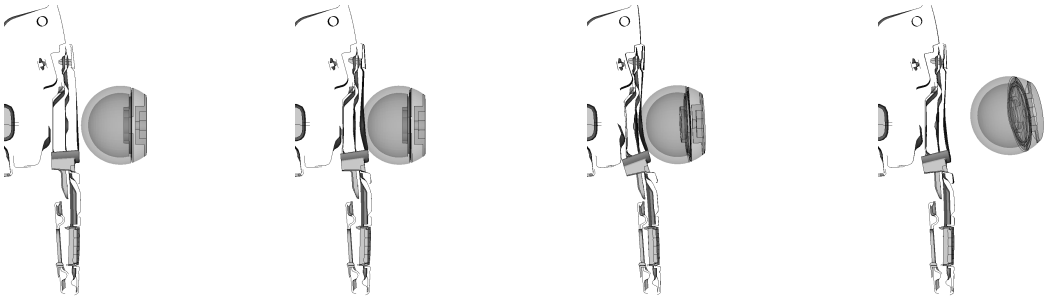

(a) T = 0 ms *(b) T = 4 ms* *(c) T = 15 ms* *(d) T = 50 ms*

Figure A.15: Close-up kinematics of the headform impact for 420 mm simplified truck model height at 24 km/h.

kinematics

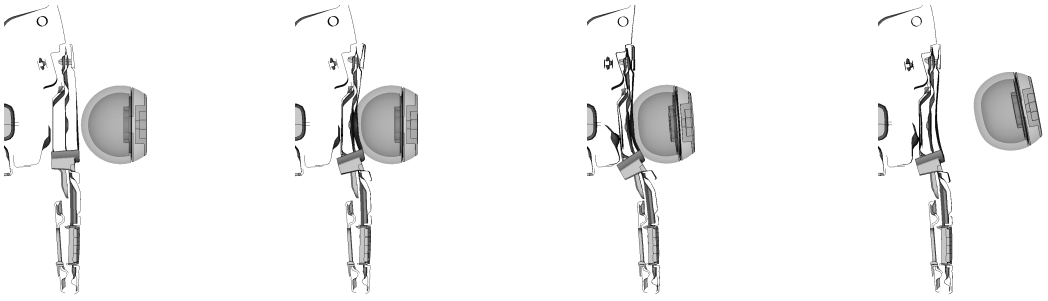

(a) T = 0 ms *(b) T = 4 ms* *(c) T = 15 ms* *(d) T = 50 ms*

Figure A.16: Close-up kinematics of the headform impact for 420 mm simplified truck model height at 40 km/h.

A.1.3 Head COG Resultant acceleration and DAMAGE Compilation

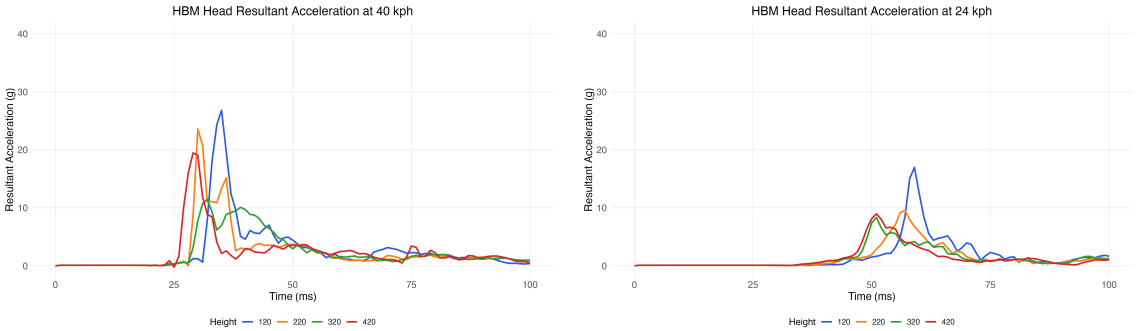

(a) Resultant Acceleration at 40 km/h **(b)** Resultant Acceleration at 24 km/h

Figure A.17: Comparison of Head COG Resultant Acceleration across varying simplified truck model heights at 40 km/h and 24 km/h impact speeds for VIVA+ 50th %ile HBM.

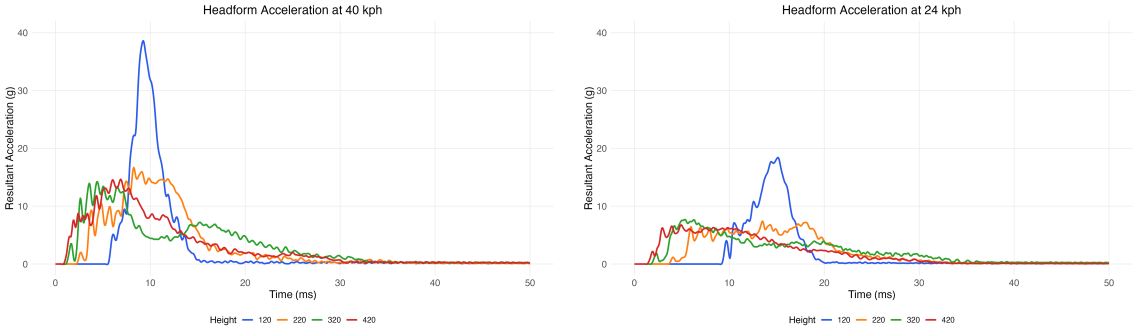

(a) Resultant Acceleration at 40 km/h **(b)** Resultant Acceleration at 24 km/h

Figure A.18: Comparison of Head COG Resultant Acceleration across varying simplified truck model heights at 40 km/h and 24 km/h impact speeds for headform

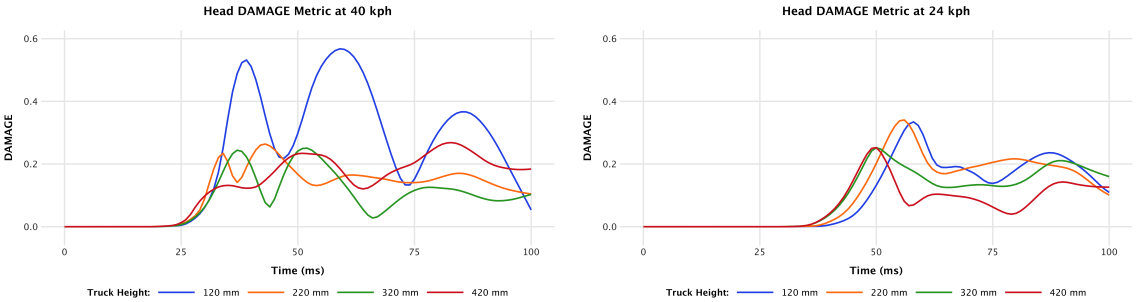

(a) DAMAGE plots at 40 km/h

(b) DAMAGE plots at 24 km/h

Figure A.19: Comparison of the Head DAMAGE metric across varying simplified truck model heights at 40 km/h and 24 km/h impact speeds for VIVA+ 50th %ile HBM.

A.2 Neck Results

A.2.1 Neck forces

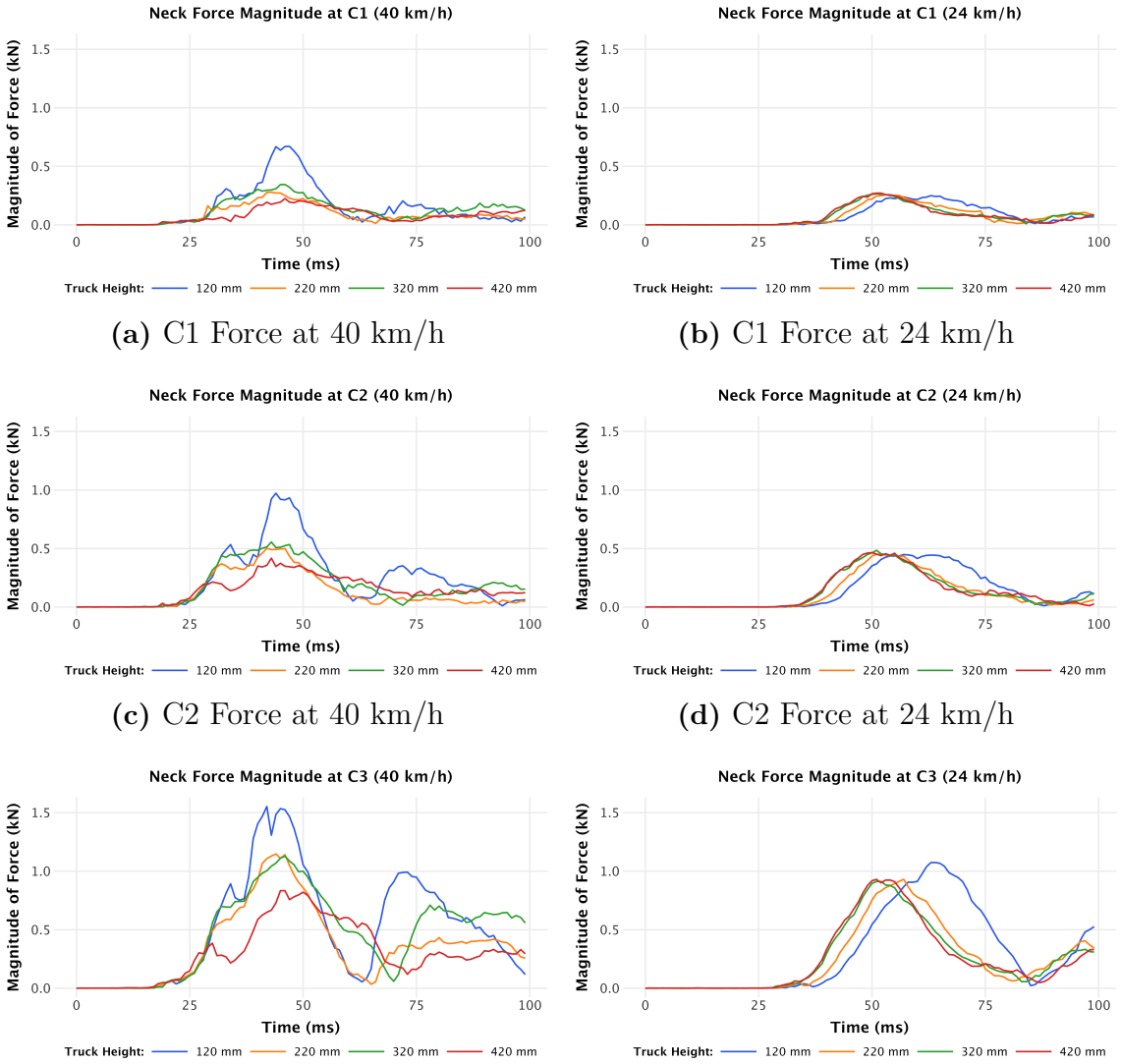

(a) C1 Force at 40 km/h

(b) C1 Force at 24 km/h

(c) C2 Force at 40 km/h

(d) C2 Force at 24 km/h

(e) C3 Force at 40 km/h

(f) C3 Force at 24 km/h

Figure A.20: Comparison of Neck Force (kN) magnitudes at the C1 through C3 cross-sections across 40 km/h and 24 km/h impact speeds.

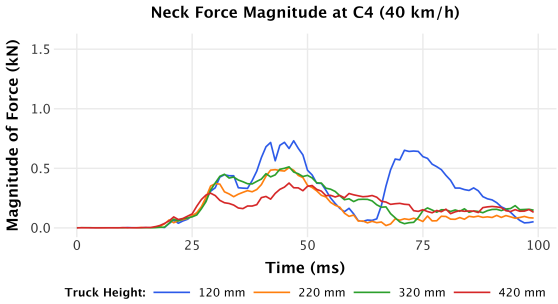

(g) C4 Force at 40 km/h

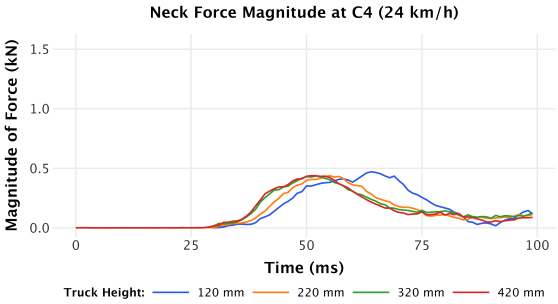

(h) C4 Force at 24 km/h

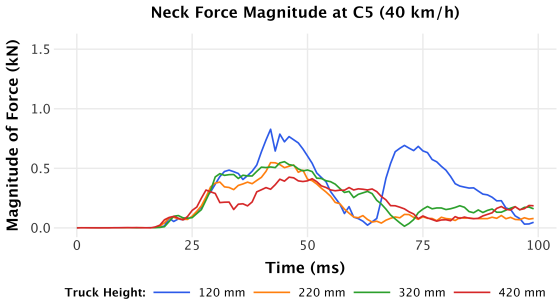

(i) C5 Force at 40 km/h

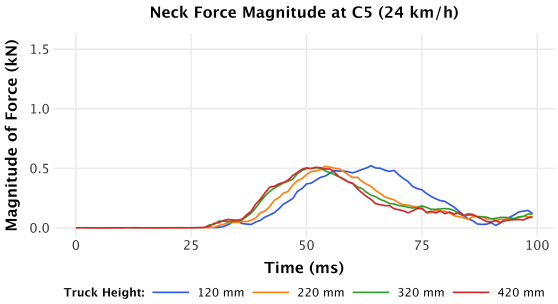

(j) C5 Force at 24 km/h

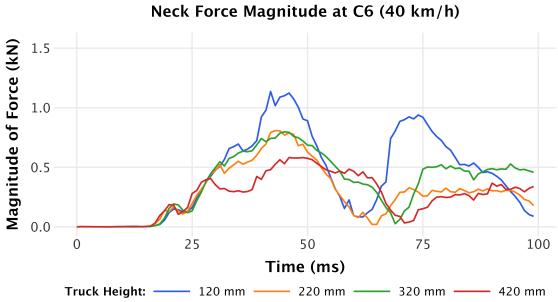

(k) C6 Force at 40 km/h

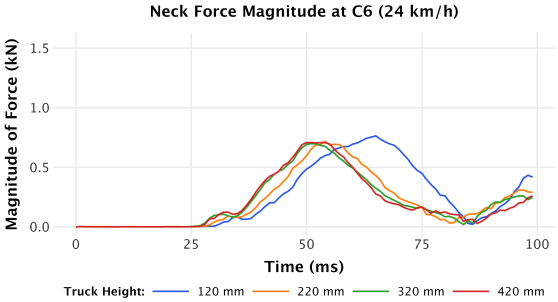

(l) C6 Force at 24 km/h

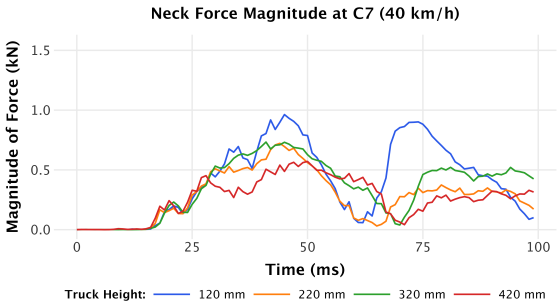

(m) C7 Force at 40 km/h

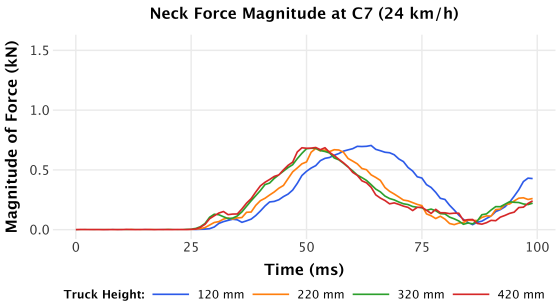

(n) C7 Force at 24 km/h

Figure A.20: Comparison of Neck Force (kN) magnitudes at the C4 through C7 cross-sections across 40 km/h and 24 km/h impact speeds. (Continued)

A.2.2 Neck Moments

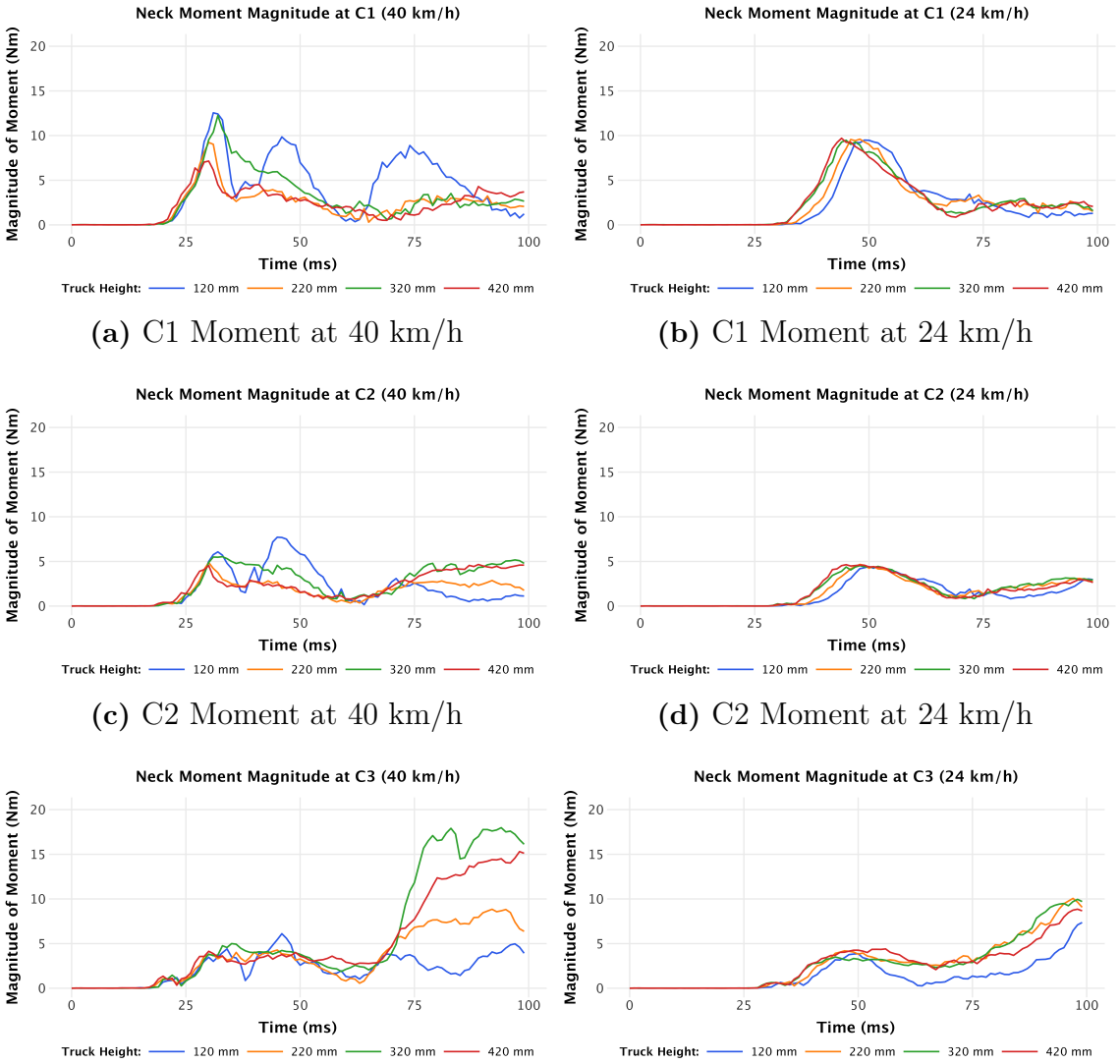

(a) C1 Moment at 40 km/h

(b) C1 Moment at 24 km/h

(c) C2 Moment at 40 km/h

(d) C2 Moment at 24 km/h

(e) C3 Moment at 40 km/h

(f) C3 Moment at 24 km/h

Figure A.21: Comparison of Neck Moment (Nm) magnitudes at the C1 through C3 cross-sections across 40 km/h and 24 km/h.

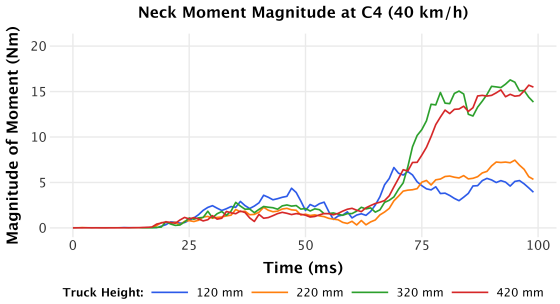

(g) C4 Moment at 40 km/h

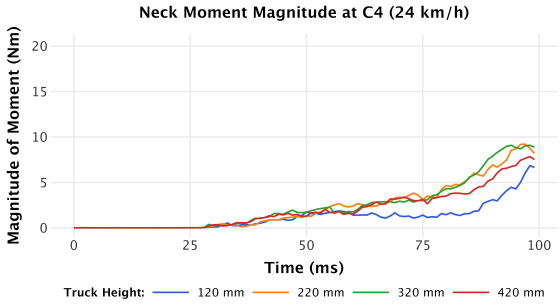

(h) C4 Moment at 24 km/h

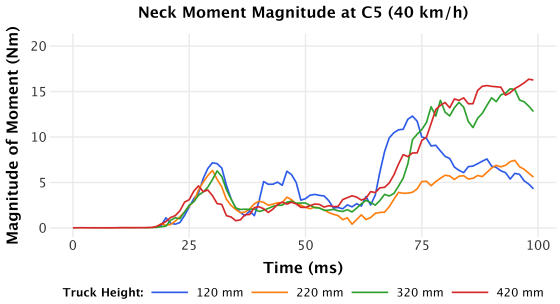

(i) C5 Moment at 40 km/h

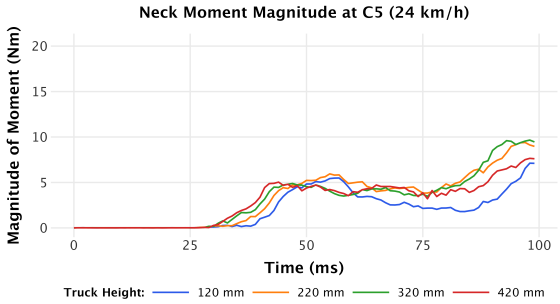

(j) C5 Moment at 24 km/h

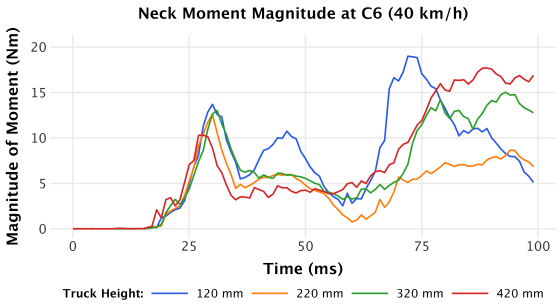

(k) C6 Moment at 40 km/h

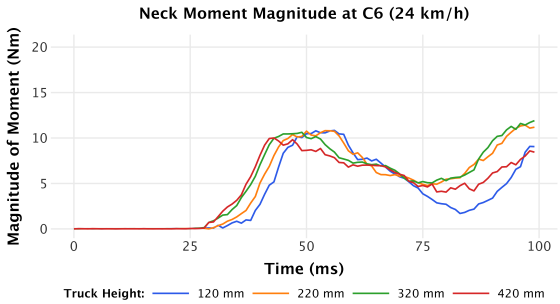

(l) C6 Moment at 24 km/h

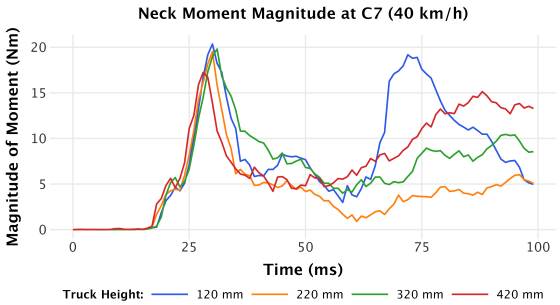

(m) C7 Moment at 40 km/h

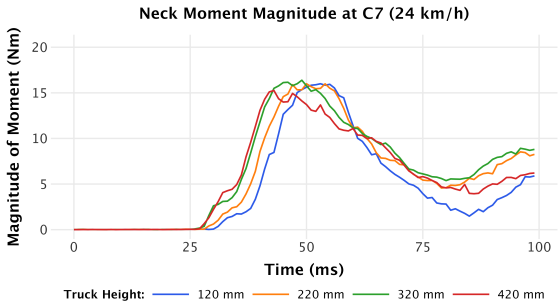

(n) C7 Moment at 24 km/h

Figure A.21: Comparison of Neck Moment (Nm) magnitudes at the C4 through C7 cross-sections across 40 km/h and 24 km/h. (Continued)

DEPARTMENT OF SOME SUBJECT OR TECHNOLOGY
CHALMERS UNIVERSITY OF TECHNOLOGY
Gothenburg, Sweden
www.chalmers.se



CHALMERS
UNIVERSITY OF TECHNOLOGY